Characteristics of the local interstellar hydrogen determined from PROGNOZ 5 and 6 interplanetary Lyman-alpha line profile measurements with a hydrogen absorption cell

Jean-Loup Bertaux, Rosine Lallement, V. G. Kurt, E. N. Mironova

Astron. Astrophys. 150, 1–20 (1985)

ASTRONOMY AND ASTROPHYSICS

Characteristics of the Local Interstellar Hydrogen determined from PROGNOZ 5 and 6 interplanetary Lyman α line profile measurements with a hydrogen absorption cell

J.L. Bertaux [1], R. Lallement [1], V.G. Kurt [2], and E.N. Mironova [2]

[1] Service d'Aéronomie du CNRS, B.P.3, F-91370 Verrières-le-Buisson, France
[2] Space Research Institute (IKI), Academy of Sciences of USSR, 84/32 Profsoyouznaya, SU-117810 Moscow, USSR

Received October 3, 1984; accepted March 21, 1985

Summary. The flow of interstellar hydrogen atoms in the solar system was observed through resonance scattering of solar Lyman α photons with two Lyman α photometers placed on board PROGNOZ 5 and PROGNOZ 6 soviet satellites, placed on high apogee orbits in 1976 and 1977. These photometers were equipped with a hydrogen absorption cell, which allowed the study of the spectral profile of the scattered interplanetary Lα emission, and hence the velocity distribution of H atoms. After subtraction of a small geocoronal contribution, the data collected at five different locations in the solar system were compared to a model of the interstellar H flow, modified by the solar interaction. From this comparison, five parameters describing atomic hydrogen of the Local Interstellar Medium (LISM) and two parameters describing the solar interaction could be simultaneously derived to give a good fit of the upwind hemisphere. The downwind hemisphere could not be fitted so well, probably because of heliosphere perturbations not accounted for in the model. The solar Lα flux at line center was determined, as well as the ionization rate of H atoms.

The direction of the hydrogen flow is quite similar to the one determined earlier for helium atoms with the same instrument: $\lambda_0 = 71 \pm 2°$, $\beta_0 = -7.5 \pm 3°$ in ecliptic coordinates, whereas the velocity V_w is $20 \pm 1\ \mathrm{km\,s^{-1}}$, instead of $27 \pm 3\ \mathrm{km\,s^{-1}}$ for the helium atoms.

The LISM temperature is found to be $T = 8000 \pm 1000$ K and the LISM H density is in the range 0.03 to 0.06 atoms $\mathrm{cm^{-3}}$. When compared to the He density of 0.015 to 0.02 atoms $\mathrm{cm^{-3}}$, it suggests that the LISM is substantially ionized ($\simeq 70\%$).

It can be concluded that the solar system is presently embedded in a hot, tenuous and partially ionized region of the LISM. In the general description of the physical state of interstellar matter by McKee and Ostriker, it corresponds to the phase characteristics of an interface region, located between a cold and dense cloud and a very hot and totally ionized region. The solar system would therefore be within a few parsecs of a dense cloud.

Since the direction of the H flow is different from the solar system motion respective to the local standard of rest, it can be calculated that there is an interstellar wind blowing (in this frame of reference) at $16 \pm 1\ \mathrm{km\,s^{-1}}$ in the direction $\alpha = 14 \pm 3°$, $\delta = 66.5 \pm 3°$, or in galactic coordinates: $l_{II} = 124 \pm 3°$, $b_{II} = 4 \pm 3°$, significantly different from the direction $l_{II} = 169°$ found by Crutcher (1982) from the study of interstellar absorption lines on stars within $\simeq 100$ pc, pointing to a very local significance of this flow, justifying the concept of a Very Local Interstellar Medium (VLISM).

Key words: interplanetary Lyman alpha – interstellar wind – LISM – interstellar hydrogen

Send offprint requests to: J.L. Bertaux

1. Introduction

Studies of the Local Interstellar Medium (LISM) have greatly benefited in the last 12 years from the high resolution EUV spectrometer flown on *Copernicus*. The Lyman α absorption profile detected in the continuum spectra of O and B stars yielded information on the average hydrogen density within 10 to 70 pc from the Sun (e.g. Bohlin et al., 1978). In the range 1.3 to 5 pc, the Lyman α emission line of cooler type stars are only partially absorbed, yielding an average atomic hydrogen neutral density of $n_H \simeq 0.1\ \mathrm{cm^{-3}}$ (Moos et al., 1974; Dupree, 1975; McClintock et al., 1976).

More locally, the LISM can be probed directly in the solar system. The motion of the Sun respective to the Very Local Interstellar Medium (VLISM) results in a permanent flow of interstellar gas, which manifests itself by resonance scattering of solar H Ly α (121.6 nm) and He (58.4 nm) photons.

This interstellar/interplanetary hydrogen was first observed and recognized as resulting from an "interstellar wind" through the mapping of extraterrestrial H Ly α emission (Bertaux and Blamont, 1971; Thomas and Krassa, 1971).

The study of this flow in the solar system can yield the characteristics of the local interstellar medium provided that the interaction between the Sun and the flow is well understood, and that diagnostic measurements are made.

The solar interaction modifies the spatial and velocity distribution of the VLISM gases in the vicinity of the Sun, and creates a non-isotropic pattern of backscattered UV radiation of He 58.4 nm and H Lyman α. Models have been described by Blum and Fahr (1970), Axford (1972) and later reviews by Fahr (1974), Thomas (1978), and Holzer (1977). Atoms are moving along hyperbolic orbits in the gravitational field of the Sun. Partial losses are suffered through ionization by solar EUV photons, electron

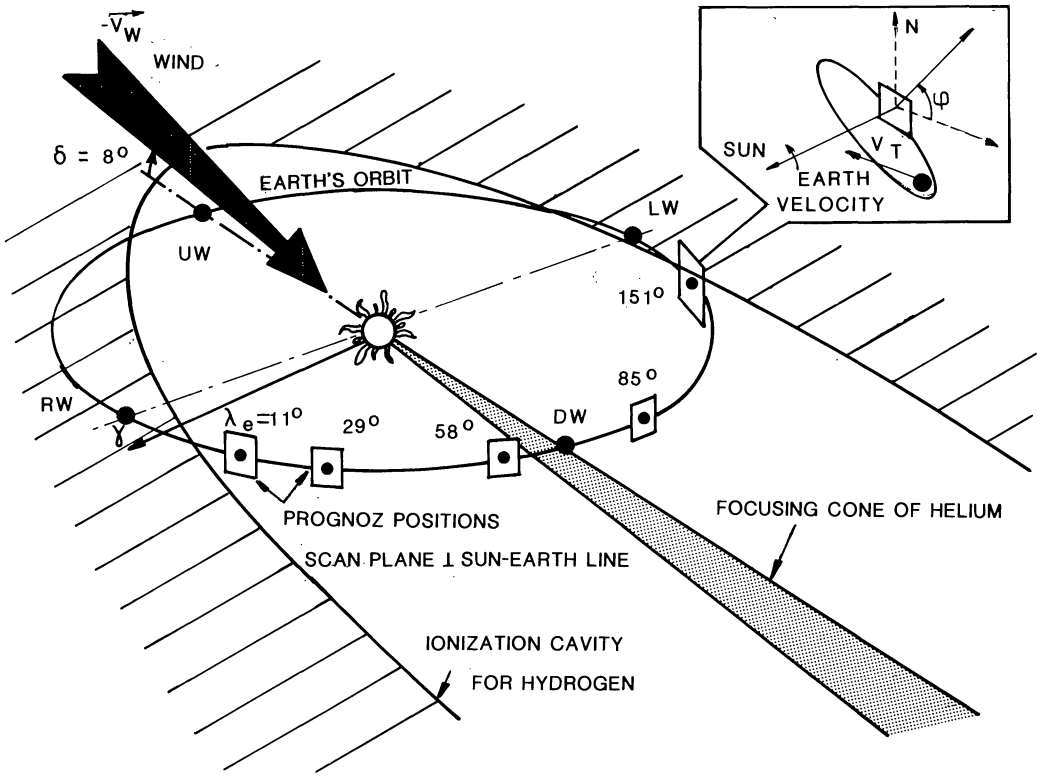

Fig. 1. The position of PROGNOZ (in orbit around the Earth) are indicated in the solar system for the five observations S_1 to S_5, and defined by the Earth's ecliptic longitude λ_e. The flow of interstellar gas $-V_w$ results in a focusing cone of helium and in a ionization cavity for hydrogen, elongated in the downwind region. Four particular positions UW, RW, DW, LW (respectively upwind, right of wind, downwind, left of wind) are sketched in the solar system. The plane of observation is perpendicular to the Sun-Earth line, and the angle ϕ determining a particular direction of sight is measured from the direction opposite to the orbital Earth's Velocity: $\phi = 90°$ toward the North Ecliptic Pole, $\phi = 270°$ toward the South Ecliptic Pole

impact and charge exchange with solar wind protons. For H atoms, the solar Ly α radiation pressure F_r compensates more or less the solar gravitation F_g, and the parameter $\mu = F_r/F_g$ depends on the solar activity.

All hyperbolic orbits of Helium atoms cross the downwind axis (opposite to the vector V_w, defining the direction of the sun motion respective to the LISM, *from where* comes the wind), creating a spectacular cone of gravitational focusing around this axis.

The shape of this cone, along with the whole He I 58.4 nm photometric pattern, was observed with PROGNOZ 6 experiment, and compared recently with an interaction model by Dalaudier et al. (1984), which derived the characteristics of interstellar helium in the vicinity of the sun. Their results will be compared in the last section to the hydrogen characteristics determined in the present paper.

On the contrary, both radiation pressure and ionization prevents H atoms to focus in the downwind zone, which is partially void of hydrogen.

The different behaviour of He and H atoms is schematically illustrated in Fig. 1, where the focusing cone of Helium and the "ionization cavity" boundary are represented.

The downwind region would be totally void of hydrogen, if the LISM temperature T was very low and all atoms would have the same velocity vector $-V_w$ (cold model) and if μ was $\geqq 1$. But it was recognized rather early (Bertaux et al., 1972) that T was at least 1000 K, from the fact that there was still a substantial Ly α emission coming from the downwind direction.

One could therefore think that the temperature T could be determined from the Lα emission photometric pattern. However, other parameters (V_w, μ, the ionization rate β) are also controlling the shape of the cavity. In a companion paper by Lallement et al. (1984) it is shown through modeling that nearly identical Lα intensity distributions can be obtained with quite different values of these parameters, if combined adequately. Therefore, the sole photometric pattern cannot provide a good diagnostic for these parameters, whereas the study of the velocity distribution of H atoms can discriminate them.

Since the solar Lyα line is spectrally quite large and assuming as a first approximation it is flat around its center, all atoms are excited at the same rate, whatever is their velocity, and thanks to Doppler effect the interplanetary Lyman α spectral profile is the exact image of their velocity distribution (projected on the line of sight, integrated and properly weighted along the line of sight).

The temperature T can be readily derived from the linewidth, and V_w can be determined from the Doppler shift measured in several different directions. However, a very high spectral resolution is needed ($\simeq 10^{-3}$ nm or better), together with a good photometric sensitivity. With the EUV high resolution spectrometer of *Copernicus*, Adams and Frisch (1977) obtained a weak line of the LISM H Ly α emission, in only one direction of sight after six days of observations. They found a Doppler shift of 22 ± 3 km s^{-1} and a width corresponding to 20,000 K or less.

A different experimental approach was set up 12 years ago, when we decided to build a light-weight, highly sensitive photometer, associated with a resonance-absorption cell, as a part of the payload of two scientific satellites, PROGNOZ 5 and PROGNOZ 6, in the frame of the french-soviet cooperation. The H hydrogen absorption cell can be used as a very high resolution

"negative" spectrometer (stopping all photons within $2\ 10^{-3}$ nm from Lyman α wavelength 121.566 nm), the spectral scanning being provided by a spatial scanning, which modulates the Doppler shift according to the observation geometry.

In this paper we present the final analysis of this investigation on the characteristics of hydrogen in the LISM. Two principal difficulties had to be overcome in order to achieve this goal. One is that, even at 200,000 km of distance from Earth's center, there was still some Lα emission coming from the geocorona (this huge cloud of H atoms populating the Earth's exosphere), superimposed on the interplanetary emission we were supposed to study. The other is that the velocity distribution of H atoms, starting as a Maxwell Boltzmann distribution at a large distance from the sun, is modified by several effects of solar interaction which had to be carefully modeled in order to retrieve the dynamical parameters T and V_w from the measurements.

Notwithstanding these difficulties, a first estimate of $T = 8800 \pm 1000$ K was published (Bertaux et al., 1977) soon after the launch of PROGNOZ 5. In this early analysis, we had selected observations taken at apogee, in a direction opposite to the Earth where geocoronal contamination was certainly small, and therefore ignored. We also assumed than the velocity distribution was *not* modified by solar interaction, arguing that, when $\mu = 1$, solar Lα radiation pressure counter balances gravitation and all H atoms trajectories are straight lines followed at a uniform velocity (a case referenced as the uniform gaussian case). This estimate was later corrected by Wu and Judge (1980), who re-interpreted our measurement with a more sophisticated model, taking into account the modification of the velocity distribution by ionization and $\mu \neq 1$. However, they had only one single measurement in their hands, and were obliged to fix the parameters β (ionization rate) and μ at estimated values. In the present analysis, since we have 5 seances of observations at various places in the solar system, we were able (by comparison with our own interaction model) to determine simultaneously the dynamical parameters T, V_w *and* the values of β and μ. As a bonus, we found definite evidence that the ionization rate by solar wind charge exchange was lower at high heliographic latitudes, implying most likely a lower solar wind mass flux (Lallement et al., 1985b).

The use of a hydrogen absorption cell for the analysis of interplanetary Lα line profile, the theory of the Doppler Angular Spectral Scanning (DASS) method, and the way to retrieve T and V_w from a limited series of measurements were described in Bertaux and Lallement (1984), in the uniform Gaussian case.

The DASS method was applied to a set of PROGNOZ measurements, and without any modeling it was demonstrated that the *local* temperature of interstellar H gas in the solar system depended on the location, as predicted in particular by Wu and Judge (1980), owing to perturbations of the velocity distribution by solar interaction (Lallement et al., 1984). Therefore, a computer code was elaborated to take into account these perturbations, and the effect of the various parameters T, V_w, β and μ was separately and systematically studied on the quantities which are actually measured with PROGNOZ experiments: the distribution $I(\phi)$ and $R(\phi)$ respectively of the Lα intensity and reduction factor in a plane perpendicular to the Earth-Sun line, for various locations in the solar system. (The reduction factor R is the factor by which the measured intensity is reduced, when a fraction of it is absorbed in the activated hydrogen cell).

From this systematic study published in this issue as a companion paper (Lallement et al., 1985a), a strategy was elaborated to sequentially determine the various parameters from a comparison with the model predictions, and the results of this exercise with PROGNOZ data is the final output of the present paper.

We must at this stage emphasize an important conclusion of our work. After a systematic exploration of all parameters, we could not find a single set of parameters which could reproduce perfectly the data everywhere. There was always a small, but significant discrepancy between the data and the model at some place, showing that the "classical" theory of the interaction between the sun and the interstellar gas (which includes gravity, Lyman α radiation pressure, and ionization by EUV and solar wind charge exchange) does not fully represent the reality.

Basically, we could not fit simultaneously the data collected toward the upwind hemisphere and the downwind hemisphere. The global fit was however better when the upwind hemisphere was well fitted. Since it is the region of sky where the interstellar H has not yet fully interacted with the Sun, it is certainly where the velocity field is the most representative of the interstellar wind parameters. Indeed, in a preliminary analysis of Prognoz results (Lallement et al., 1984), there was already an indication that the downwind region was more perturbed than predicted by the "classical" theory, as will be discussed later. For these three reasons, we have restricted our criteria of fitting to the upwind hemisphere, for the determination of the interstellar wind parameters. Thus, examination of Figs. 11–14 requires to distinguish between the fitted upwind region ($-90° \leqq \phi \leqq +90°$ for S_1

Table 1. PROGNOZ mission and observations characteristics

	PROGNOZ 5	PROGNOZ 6
Launch date	Nov. 25, 1976	Sept. 22, 1977
Orbital eccentricity e	0.9328	0.9337
Orbital period (days)	3.96	3.94
Distance apogee from Earth-center (km)	206,000	205,000
Distance of perigee from Earth-center (km)	7,160	7,030
Observations	S_5	S_1, S_2, S_3, S_4
Earth's ecliptic longitude	151°	11°, 29°, 58°, 85°,
Date of observation (1977)	2/20	10/4, 10/22, 11/15, 12/16

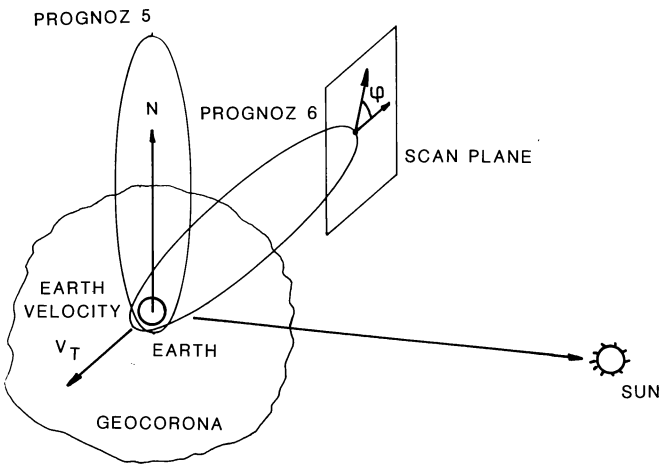

Fig. 2. Configuration of PROGNOZ orbits, the geocorona and the scan plane perpendicular to the Earth-Sun line. The inclination of PROGNOZ 6 orbit allowed to observe simultaneously the North (N) and South ecliptic regions without too much interference from the geocorona

to S_3 and $90° \leqq \phi \leqq 270°$ for S_4 and S_5) and the unfitted downwind hemisphere.

2. Mission and experiment description

Devoted entirely to the scientific study of space, soviet satellites PROGNOZ 5 and 6 were launched respectively on November 25, 1976 and September 22, 1977 on highly eccentric orbits, which characteristics are given in Table 1. Each of them returned scientific data over slightly more than three months, the Earth describing a quarter of its orbit in the mean time.

The spacecraft were spin-stabilized, the spin axis being every few days re-aligned with the Sun direction, and the spin rate being about 3° per second. Between two pointing manoeuvers, the spin axis kept roughly a fixed inertial position. The optical axis of the Lyman α photometer was placed at 90° from the spin axis, providing a scan of the celestial sphere along a great circle approximately (within a few degrees) perpendicular to the Sun-Earth line.

The line of apsides was differently inclined for the two missions, respective to the ecliptic plane: nearly 90° for PROGNOZ 5, and ~50° for PROGNOZ 6. As a result, the South ecliptic region was more or less permanently masked by the Earth and the bright inner geocorona for PROGNOZ 5 when it was around its apogee, whereas for PROGNOZ 6 both North and South ecliptic regions could sometimes be observed (Fig. 2) simultaneously.

The whole instrument weighted 7 kg and consisted of four UV–EUV photometers channels. Three of them were devoted to He I 58.4 nm and He II 30.4 nm radiation. No significant contribution from He II 30.4 nm was recorded (except when the sunlit Earth crossed the field of view). The He I 58.4 nm data has been analyzed in detail (Dalaudier et al., 1984), yielding the characteristics of interstellar Helium.

The Lyman α channel is presented schematically in Fig. 3. An optical baffle was used to eliminate stray light, the entrance of which was anyway placed in a shadowed area of the spacecraft. The hydrogen absorption cell, a glass vessel 8 cm long with two MgF_2 windows, was serving a double purpose: the very selective absorption of Lα photons, and the optical definition of the photometer. The entrance window of the H_2 cell was a lens of 16 mm useful diameter, and focal length 105 mm, at the focus of

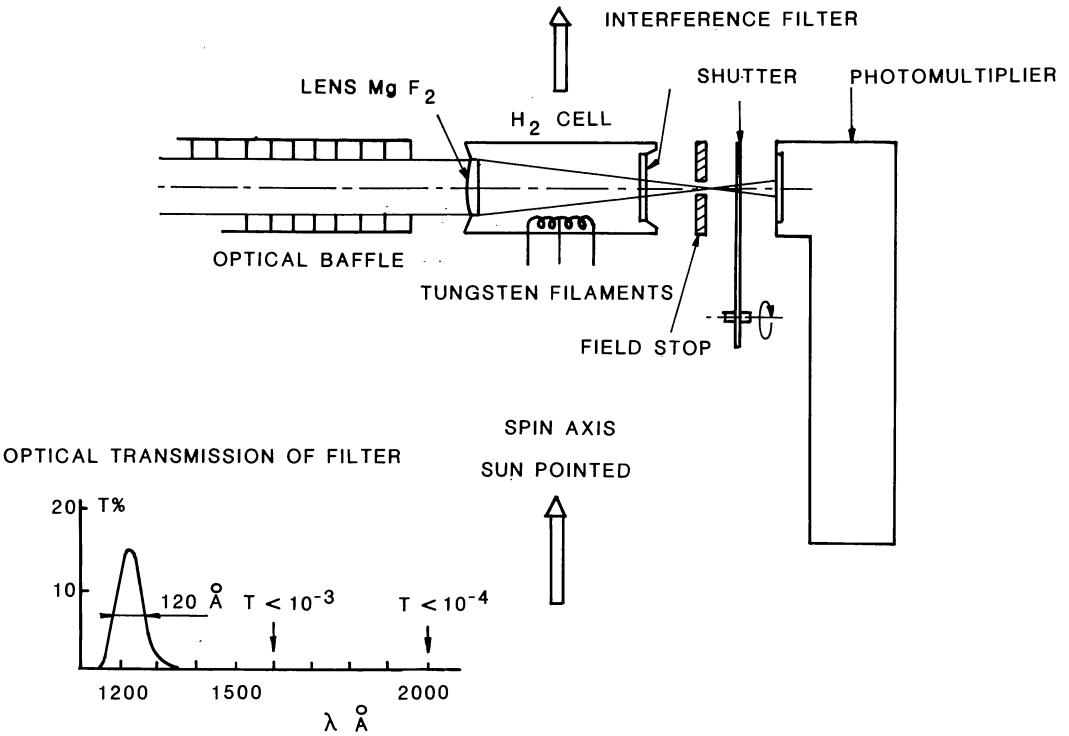

Fig. 3. Optical design of the Lyman-alpha channel. The hydrogen cell is placed in front of the photomultiplier. A UV filter is deposited on the back side of the exit window of the cell. The transmission of the interference filter is indicated in the lower left corner. The optical axis is perpendicular to the rotation axis, maintained toward the Sun

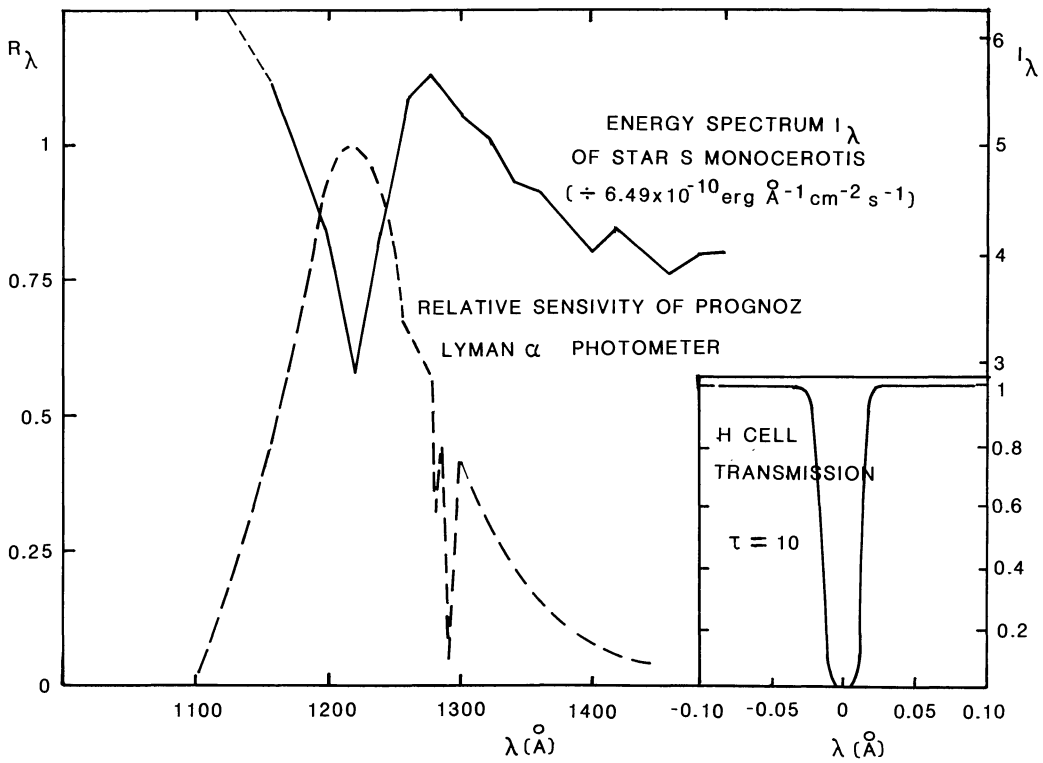

Fig. 4. The relative dependence of the overall efficiency $R_\lambda = Q_\lambda T_\lambda$ of the photometer is represented as a function of wavelength λ (dashed line). The "hole" just below 1300 Å is an effect of the interference filter. Maximum efficiency is around Lyman-alpha. The energy spectrum of S Monocerotis, a bright UV star (solid line), was multiplied by the efficiency curve to determine the absolute calibration of the photometer from repeated observations of this star. Five other stars were also used. In the lower right corner is displayed the transmission curve of the H absorption cell when the optical thickness $\tau = 10$ is created inside the cell by heating a tungsten filament, as a function of $\Delta\lambda = \lambda - \lambda_0$, λ_0 central Ly α wavelength

which (behing the cell) was placed a rectangular hole defining the field-of-view of $1.1° \times 2.7°$, the length being along the FOV motion during the spacecraft rotation. On the exit window of the H_2 cell had been vacuum deposited a UV interference filter, isolating approximately a bandwidth of $\simeq 12$ nm around Lα (121.6 nm). The overall transmission of the cell was about 7% at Lα.

A shutter blade was placed between the field stop and the photomultiplier (PM) window. Closed at regular intervals, it showed that the PM dark counting rate was usually a few counts (3 to 8) per second, except when crossing the radiation belts (where it could reach 40 10^3 counts s^{-1}) and during one occasion, in October 1977. Though at this time the spacecraft was near the apogee, far outside the magnetopause, it was hit by a flow of Mev protons coming from a major solar eruption, and the dark counting rate reached about 100 per second.

The detector was a side-window (MgF_2) photo multiplier with a "solar blind" potassium bromide (KBr) cathode, with a high quantum efficiency $Q \simeq 20\%$ at Lα.

The PM was used in a pulse-counting mode. The counting time being 1.03 s, the actual FOV was larger than the instantaneous FOV by about 3°, leading to a total FOV of $1°1 \times 5°$. The solid angle of the static FOV was $\Omega = 1\ 10^{-3}$ steradian.

The overall variation of the sensitivity as a function of wavelength was measured in the laboratory before launch, yielding the relative curve $Q_\lambda T_\lambda$ indicated in Fig. 4, together with the spectrum of the bright hot star S Monocerotis. Repeated observations of this star and others (which absolute flux is known from other measurements) during flight allowed an in-flight calibration of the instrument. Thanks to its simplicity, the sensitivity of this Lα photometer was very high: 3.5 counts per counting time (1.03 s) for an intensity of 1 Rayleigh

$$\left(1\,\text{Rayleigh} = \frac{10^6}{4\pi}\,\text{phot cm}^{-2}\text{s}^{-1}\text{ster}^{-1}\right)$$

for PROGNOZ 6, and 1.5 counts per Rayleigh for PROGNOZ 5.

Before reaching the PM tube, Lα photons are passing through the absorption cell, which contains a low pressure (0.3 Torr) of H_2, totally transparent to Lyman α. In such state, the cell is OFF and the measured intensity is called I_{OFF}. When a couple of tungsten filaments are electrically heated inside the cell, H_2 is dissociated in H atoms and an optical thickness τ_0 (at line center λ_0 of Lα) is created; $\tau_0 = 8$ and 10 respectively for PROGNOZ 5 and 6. Photons whose wavelength is lying within ~ 1.5 picometer (0.015 Å) are scattered by H atoms inside the cell in all directions, and absorbed on the wall of the cell. When the cell is activated (ON), the measured intensity I_{ON} is smaller than I_{OFF} by the reduction factor $R = I_{ON}/I_{OFF}$.

The exact transmission function of the H cloud inside the cell is displayed in Fig. 4; it is nearly a rectangular profile, with a transmission $e^{-10} \simeq 0$ inside the rectangle, and 1 outside the rectangle. As explained in Bertaux and Lallement (1984), for a Gaussian profile of the interplanetary emission at temperature T, the reduction factor R can be readily calculated as a function of T and the Doppler shift $\Delta\lambda = \lambda_0 \frac{V_D}{c}$ between the emission and the photometer. Of course, the radial relative velocity V_D depends on the looking direction; the reduction factor reaches a minimum value R_{min} when $V_D = 0$ (no Doppler shift, maximum absorption)

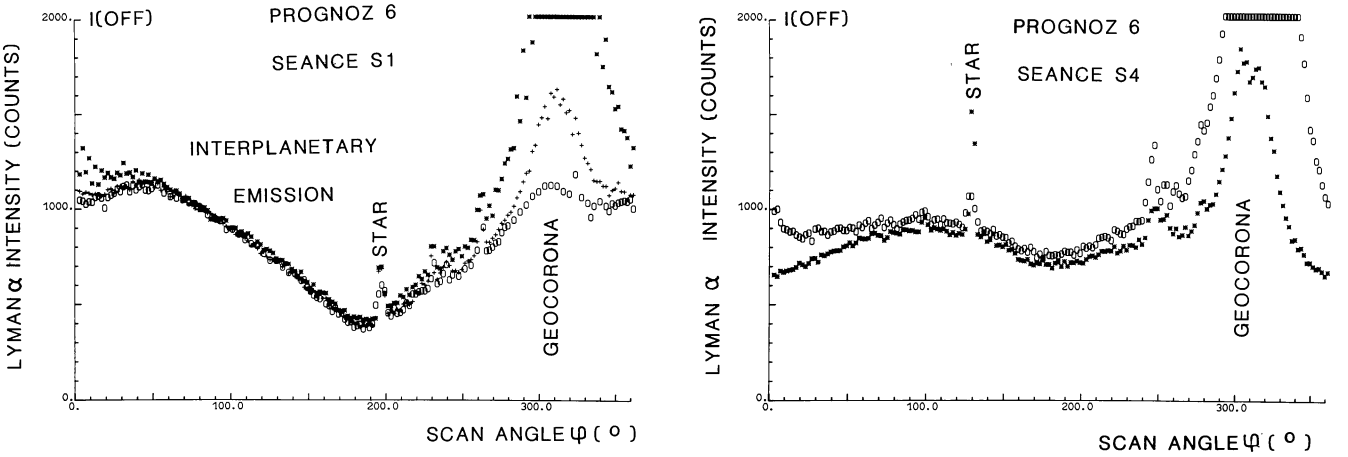

Fig. 5a. The distribution of Lyman-alpha intensity is represented as a function of angle ϕ for three different slices of observation S_1 with three different symbols. Narrows bumps are due to hot stars, whereas the wide bumps around $\phi = 310°$ are due to different slices cut through the geocorona when the spacecraft is moving along its orbit (see Fig. 17). The lower bump corresponds to a scan plane more distant from Earth's. The intensity is measured in counts per 1.03 s (counting time). The H cell is not activated. The plot has been restricted for intensities lower than 2,000 counts, but measurements were never saturated. From 50° to 150° the measured signal is practically not contaminated by geocorona and the variation is due to the interplanetary emission pattern. The sensitivity of the instrument was estimated to be 3.5 count per Rayleigh. **b** Same as **a**, for two slices of observation S_4. In this seance, there is more geocoronal signal in all directions ϕ for one slice than for the other

and may reach unity (no absorption) if the Doppler Shift is larger than the width of the emission line. Curves of R as a function of T and V_D for $\tau_0 = 10$ where given in Bertaux and Lallement (1984), for the H cell temperature of 300 K.

3. Observations

When operated, the instrument was measuring the intensity during 1.03 s every 10 s, alternatively with the H cell ON and OFF, in a non-synchronized fashion with the spin angle ϕ, describing in the scan plane the angle of the direction of sight with the vector opposite to the Earth's velocity (Fig. 1). $\phi = 90°$ for the North Ecliptic pole and $\phi = 270°$ for the South ecliptic pole.

In order to establish the distribution of intensities $I_{\mathrm{OFF}}(\phi)$ and $I_{\mathrm{ON}}(\phi)$ in a plane, six hours of data were averaged together in bins of $\Delta\phi = 2°$; the very small dark counting rate was then subtracted. About 10 measurements were averaged together in each bin. In Fig. 5a is represented the signal $I_{\mathrm{OFF}}(\phi)$ for three consecutive periods of 6 h. The three curves are quite similar, except for a bump around $\phi = 300°$, which corresponds to the geocoronal emission superimposed on the interplanetary emission. Smaller bumps are due to hot stars, all identified.

When the spacecraft was moving along its orbit, the scan plane was cutting different slices of the geocorona (nearly spherically symmetric). The lower bump was corresponding to a scan plane whose distance to the Earth's center was 7 10^4 km, whereas for the larger bump this distance was only $\sim 2\ 10^4$ km. In order to minimize the geocoronal contamination, we restricted the present analysis to observations performed when the spacecraft was at a distance larger than 10^5 km from the Earth. Still, for a 4 days orbital period, the time spent around the apogee was quite large, and 5 to 10 "slices" of 6 h duration each were obtained during one single orbit, which represent one set of measurement, referred to as one observation in the following. The ecliptic longitude of the Earth during observations S_1, S_2, S_3, S_4 of PROGNOZ 6 and S_5 of PROGNOZ 5 is indicated in Table 1 and sketched in Fig. 1. In Fig. 5b are represented the curves for two slices of observation S_4, showing a somewhat different configuration of geocorona and interplanetary signal.

The problem of disentangling the geocoronal contribution I_g from the interplanetary contribution I_p was not a trivial one. We devised a method which is based upon the fact that, during one observation, during which the scan plane has a constant orientation, the interplanetary signal $I_p(\phi)$ will remain constant, whereas the geocoronal signal $I_g(\phi)$ will vary according to the position of the spacecraft in respect to the geocorona. Therefore, any measured difference $I_2(\phi) - I_1(\phi)$ between two slices can be attributed entirely to the variation of the geocoronal contribution. A geocoronal model was constructed, which was adjusted to data in order to produce model intensity variations identical to the measured one. The model was then assumed to be good enough to also predict accurately *absolute* intensities, which were then subtracted from the total measurement $I_m(\phi)$ to yield the *pure* interplanetary emission $I_p(\phi)$.

For observation S_1 of PROGNOZ 6, six slices numbered from 1 to 6 were treated in this way, and both the total and the corrected pure interplanetary signal $I_p(\phi)$ are represented in Fig. 6a–c for three of them.

The geocoronal bump, seen on all graphs around $\phi = 310°$, is increasing from slice to slice. On each graph are represented both the measured intensity I_m and the corrected intensity, representing the pure interplanetary signal I_p after subtraction of the geocoronal signal I_g, estimated according to the above mentioned procedure. For slice 1 (Fig. 6a), the difference $I_g = I_m - I_p$ is hardly noticeable and does not exceed a few Rayleigh, except around $\phi = 310°$. On the contrary, for slice 5 (Fig. 6c), I_g is noticeable everywhere, and amounts to a minimum value of $\simeq 15$ Rayleigh, even when the direction of sight is opposite to the general direction of the geocorona. When the geocoronal correction I_g exceeded 300 Rayleigh (which corresponds to about 1,100 counts for PROGNOZ 6), the correction was estimated unsafe and no value of I_p was calculated.

The six sets of I_p data points coming from the six slices are plotted together in Fig. 7 after elimination of the regions where stars passed through the field-of-view (all were identified). All six

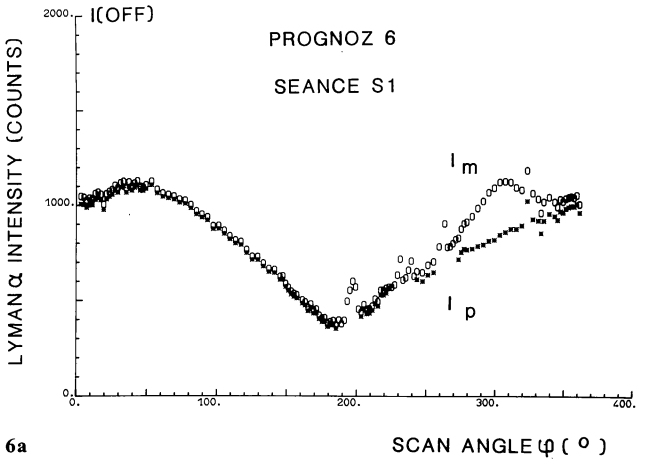

6a

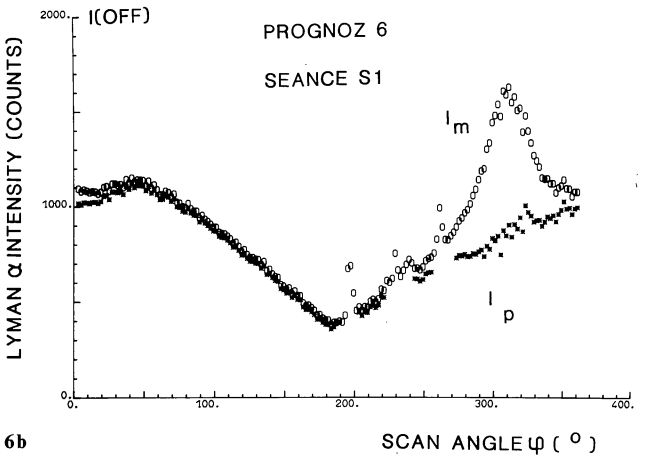

6b

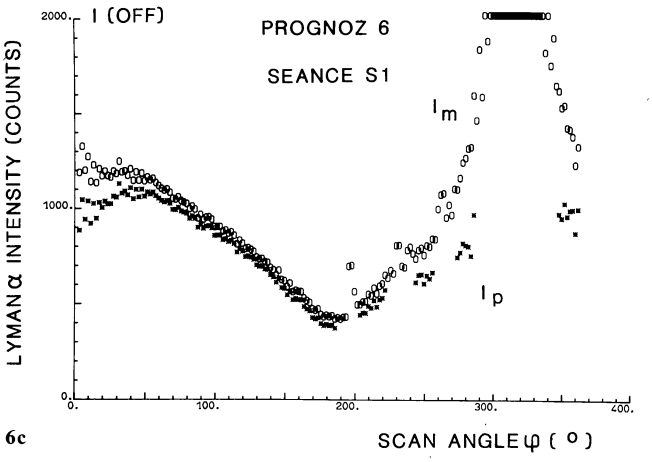

6c

Fig. 6a–c. As a result of the correction process, the contribution of the geocorona was estimated and subtracted from the measurements I_m (open symbols O) to yield the pure interplanetary emission I_p (black crosses) for three different slices of Seance S_1. No value of I_p was calculated at stellar positions or when the geocoronal signal exceeded $\simeq 300$ Rayleigh. The H cell was not activated during all these measurements

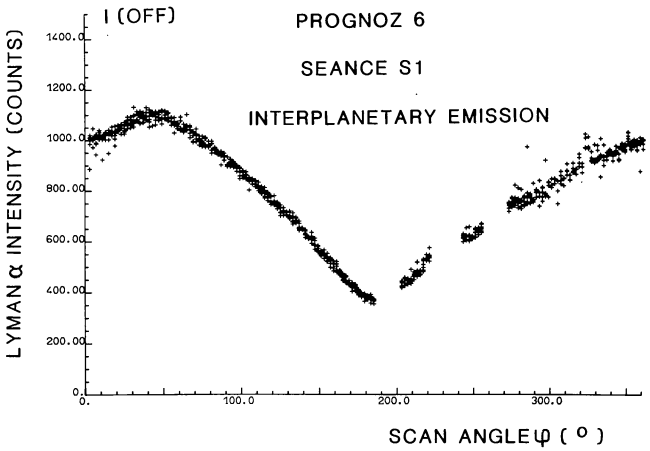

Fig. 7. The six curves $I_p(\phi)$ for observation S_1 are plotted together, to yield the pure interplanetary emission, showing very little dispersion and indicating the validity of the method of geocoronal estimation. Small sections are missing around hot stars

sets are quite similar, which indicates the validity of our geocoronal correction over the six slices to yield the nonabsorbed pure interplanetary signal $I_p(\mathrm{OFF})$ for each bin $\Delta\phi = 2°$. For each observation, at a given point in the solar system, several slices were in the same way combined together to give one single distribution $I_p(\mathrm{OFF})$.

The observation S_1 of PROGNOZ 6 was a particularly favourable one, since on the first slice the maximum geocoronal signal did not exceed $\simeq 100$ Rayleigh and the pure I_p signal could be retrieved for all directions of sight (except around some stellar positions).

This was not the case for all observations considered in the present analysis, and for some regions we have totally discarded an estimate of $I_p(\mathrm{OFF})$.

In Fig. 8 is represented for slice 2 of seance S_1 the PROGNOZ 6 measurements $I_m(\mathrm{ON})$ obtained when the H cell was operated at optical thickness $\tau = 10$, averaged and binned like the measurements $I_m(\mathrm{OFF})$, which are also represented on the graph. The geocoronal bump has completely disappeared, because, as sketched in the corner of the figure, the geocorona is much cooler than the interplanetary hydrogen, the emission line is much narrower, and besides there is no significant Doppler shift between the spacecraft and the geocorona, since measurements were collected around apogee, where the spacecraft velocity is small. At 10 Earth Radii, the effective temperature of exospheric hydrogen has been calculated to be 300 K (Bertaux, 1978), whereas, as we shall see, the interplanetary hydrogen temperature is around 8000 K.

Still, a small geocoronal signal $I_g(\mathrm{ON})$ not absorbed by the H cell could contribute to the total signal:

$$I_m(\mathrm{ON}) = I_p(\mathrm{ON}) + I_g(\mathrm{ON}).$$

One can also define a reduction factor on the geocorona:

$$R_g = \frac{I_g(\mathrm{ON})}{I_g(\mathrm{OFF})}.$$

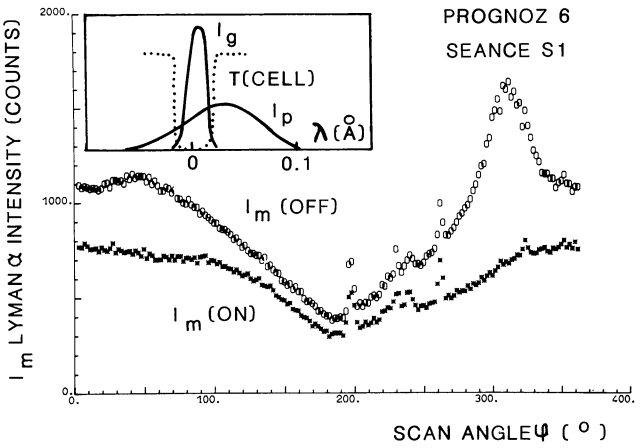

Fig. 8. The absorption effect of the H cell is illustrated by comparing the measurements I_m(OFF) to the measurements I_m(ON) when the cell is activated, for slice N° 2 of observation S_1. There is some absorption in every direction, but the geocoronal bump is totally eliminated because the geocoronal emission is cool and there is no substantial Doppler Shift as sketched in the upper left corner, where the H cell transmission is the dotted line. Around $\phi = 50°$ where there is no large geocoronal emission, the absorption of the interplanetary signal is quite important

With an appropriate exospheric model of hydrogen distribution of the type described by Chamberlain (1963), the velocity distribution and the resulting geocoronal Lα line profile were computed, as well as the reduction factor R_g expected for $\tau = 10$. This was done with a computer code set up for the interpretation of OGO-5 geocoronal observations (Bertaux, 1978). For all slices of each seance, the non absorbed geocoronal contribution $I_g(\text{ON}) = R_g I_g(\text{OFF})$ could be estimated, and subtracted from I_m(ON) to yield I_p(ON), the non-absorbed pure interplanetary signal. Then all slices for one seance were averaged together.

The computed values of R_g are generally very small ($R_g \leqq 0.10$) and the corresponding correction I_g(ON), does not exceed a few Rayleigh. Therefore the uncertainty on this correction is also quite small.

The reduction factor $R_p = \dfrac{I_p(\text{ON})}{I_p(\text{OFF})}$ of the pure interplanetary Lα signal was then computed for each value of ϕ, and the corresponding curves I_p(OFF), I_p(ON), and R_p are all displayed as a function of ϕ in Fig. 9a–e. Some points are missing where stellar or geocoronal contamination was judged to be too severe.

These curves will now serve as the data base to be compared to our model of the interplanetary Lyman α line profile, in which we are able to predict both the intensity and the reduction factor when the optical thickness $\tau = 10$ is used in a hydrogen absorption cell. The various parameters will be determined sequentially, following the strategy derived from the systematic study of the companion paper (Lallement et al., this issue).

4. Interpretation

The position of the Earth in the solar system during the five seances of observations are represented in Fig. 1, together with the helium cone of focusing. Theory predicts that gravitational focusing by the sun will induce a region of enhanced density of helium atoms along the axis V_w, in the downwind direction. Indeed such a cone was first detected by Weller and Meier (1974), and more recently by Dalaudier et al. (1984) with helium photometers placed on board PROGNOZ 5 and 6. The ecliptic coordinates of the downwind axis found by Dalaudier et al. (1984) are:

$$\lambda_w = 74.5 \pm 3° \quad \beta_w = -6 \pm 3°$$

for the downwind axis (vector $-V_w$).

In Fig. 1 is also represented the ionization cavity which is expected to be carved into the flow of interstellar hydrogen, with a void in the downwind direction partially filled in by the velocity dispersion of H atoms associated with the interstellar temperature T.

Particular positions UW, DW, LW, RW are also indicated in Fig. 1. They correspond respectively to upwind, downwind, on the left side of the wind, and on the right side of the wind. In the companion paper the theoretical intensity and reduction factor distributions in planes perpendicular to the Sun Earth line were discussed, as a function of various parameters of the model of interaction between the sun and the interstellar matter, for these particular positions.

The measured intensity curves (Fig. 9a–e) of the interplanetary Lα emission are quite consistent with the above description. For observation S_1, at $\lambda_e = 11°$ of ecliptic longitude, which is not far from the RW position, a maximum intensity (Fig. 9a) is seen around $\phi \simeq 40°$ (not far from the upwind position) and a minimum intensity is seen around $\phi = 190°$, not far from the downwind position, and vice versa for the observation S_5 at $\lambda_e = 151°$, not far from the LW positions. Therefore, the photometric pattern indicates that indeed the flow of hydrogen comes from the same general direction as the flow of helium.

There is however a peculiar behavior of the intensity distribution for observation S_4, at $\lambda_e = 85°$, near the downwind direction (Fig. 9d). One maximum around $\phi = 90°$ (toward North Ecliptic pole) is expected from the fact that the wind is blowing from slightly above the ecliptic plane, the ionization cavity being accordingly tilted. The other maximum detected around 270°, where a minimum would be expected, was a puzzle to us for quite some time, until we understood that it was the clear signature of the fact that the ionization by the solar wind charge exchange was *lower* at high latitudes than in the ecliptic plane. A non-isotropic model of the solar wind was built, and the latitude variation of the solar wind could be adjusted such as to predict intensity distributions fitting simultaneously and almost perfectly the intensity curves of the five observations (Lallement et al., 1985b), including the existence of a secondary maximum for observations made from a downwind position. A similar effect was found on Mariner 10 interplanetary Lα observations (Kumar and Broadfoot, 1978).

This non-isotropic model is axially symmetric about the sun polar axis, and the ionization rate is constant in the ecliptic plane. As a result, for the downwind position DW, the intensities in the ecliptic plane in the two opposite directions, $\phi = 0$ and $\phi = 180°$ should be equal. When the Earth is before DW ($\lambda_e \leqq \lambda_w$) we should have $I(\phi = 0°) \geqq I(\phi = 180°)$, and after DW the contrary should hold: $I(\phi = 0°) \leqq I(\phi = 180°)$.

In Fig. 10 was plotted the ratio $\dfrac{I(\phi = 180°)}{I(\phi = 0°)}$ as a function of the Earth's ecliptic longitude λ_e for the five observations, in a semi-logarithmic fashion. Points S_1, S_2 and S_3 are below 1, whereas S_4 and S_5 are above unity. A simple graphic interpolation between S_3 and S_4 points indicates that this ratio would have reached 1 for $\lambda_e = 71° \pm 2°$, indicating rather accurately the ecliptic longitude of vector $-V_w$ for the flow of hydrogen. It is quite near the ecliptic

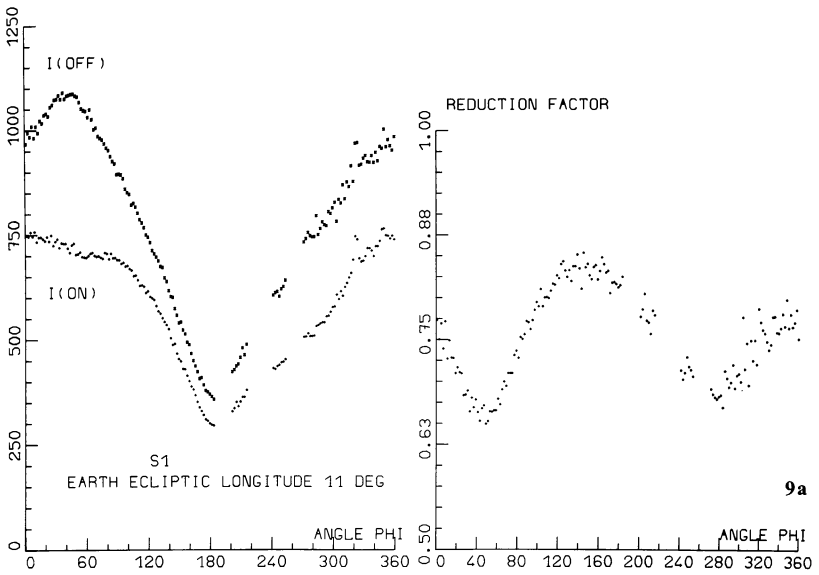

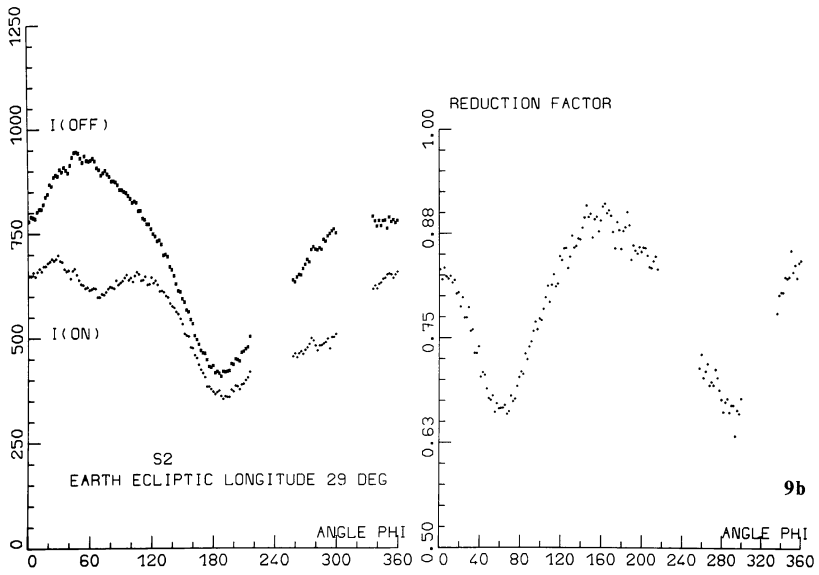

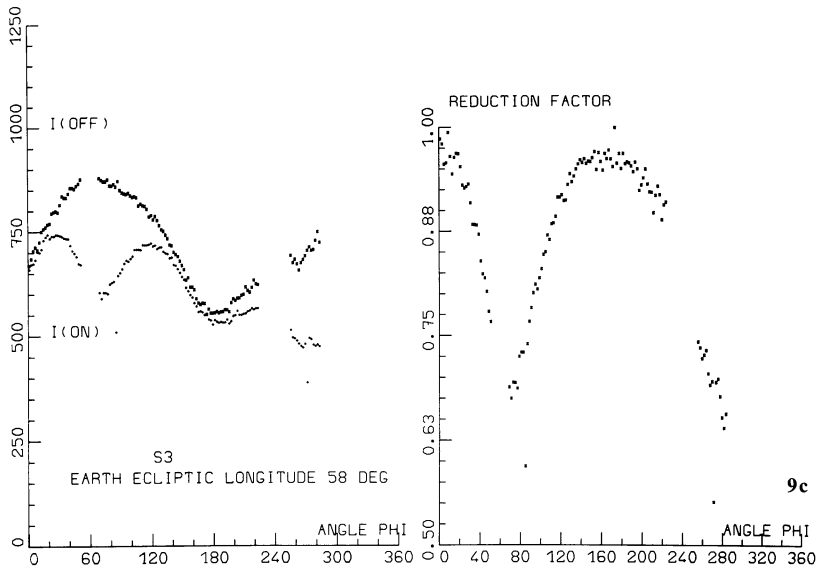

Fig. 9a–e. For the five observations S_1 to S_5, both the intensity and reduction factor of the pure interplanetary Lyman-alpha emission are shown as a function of ϕ. Both intensities I(OFF) and I(ON) have been corrected from geocoronal contamination. The ecliptic longitude λ_e of each seance is indicated. The intensity pattern I(OFF) is changing with λ_e, and governed by the upwind-downwind Lyman-alpha intensity gradient, as can be understood by placing the scans on Fig. 1. The reduction factor is governed by the angular modulation of the Doppler shift with ϕ. It shows always two minima, which width, position, and value are diagnostic of the interstellar wind parameters and its interaction with the Sun. For S_4 and S_5, there are large portions of the sky where the Doppler shift is so large that there is no noticeable absorption. The reduction factor is 1. Intensities are in counts per 1.03 as usual. The counting rate for S_5 is somewhat lower than for the other seances because of a lower sensitivity of PROGNOZ 5 instrument

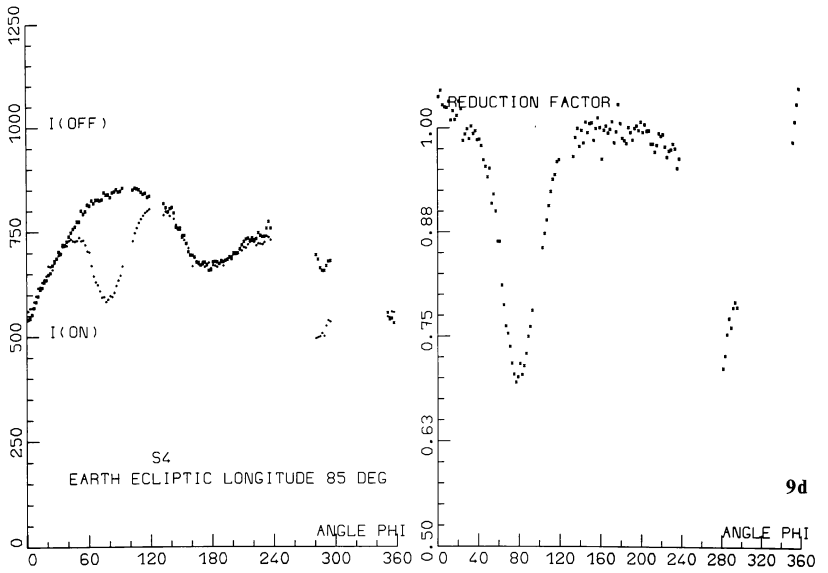

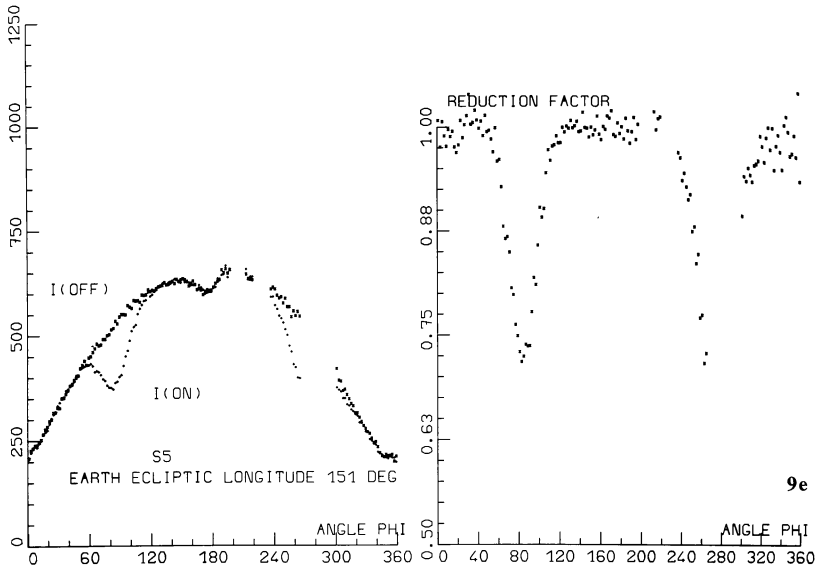

Fig. 9d and e

longitude of the helium cone, determined at $\lambda_w - 180° = 74.5 \pm 3°$ (λ_w is the ecliptic longitude of $+\boldsymbol{V}_w$).

As a preliminary conclusion, the Lyman α photometric pattern indicates an excellent agreement between the flow directions of Helium and hydrogen from interstellar origin, and in the following study of the reduction factor, the hydrogen flow direction was fixed at the helium coordinates in our model prediction of line profiles and reduction factors $R(\phi)$.

All measured curves $R_m(\phi)$ display a structure with two minima, as expected from the fact that, along a scan plane, there are two directions (opposite to each other) where the Doppler shift between the spacecraft and the hydrogen flow is zero: the absorption of the cell is centered on the emission profile, and is maximum, resulting in a minimum of the reduction factor $R_{\min}(\phi_{\min})$. The basic principles of the Doppler Angular Spectral Scan (DASS) method was described in details in Bertaux and Lallement (1984).

There is a striking difference of shape in the $R(\phi)$ curves from observation S_1 to observation S_5, the minima becoming more and more narrow. This is quite easy to understand, if one recalls that the H cell is attached to the spacecraft, itself attached to the Earth which moves at $V_T = 30\,\mathrm{km\,s^{-1}}$ in the direction $\phi = 180°$. Therefore, the total relative vector between the H cell and the interstellar H flow is $\boldsymbol{V}_r = \boldsymbol{V}_T + \boldsymbol{V}_w$ (we neglect here the orbital velocity of PROGNOZ, very small around the apogee).

For observation S_5, the vectors V_T and V_w add together around $50\,\mathrm{km\,s^{-1}}$ (assuming $V_w = 20\,\mathrm{km\,s^{-1}}$ as determined later). There is only small angular zones around $\phi = 90°$ and $\phi = 270°$ where the Doppler shift is small. Outside these zones the absorbing spectral profile is completely outside the interplanetary profile and the reduction factor is 1.

On the contrary for observation S_1, vectors V_T and V_w are of opposite sense; V_r is in the range $\simeq 10\,\mathrm{km\,s^{-1}}$, and whatever is the direction of ϕ, the Doppler shift is never too large not to absorb

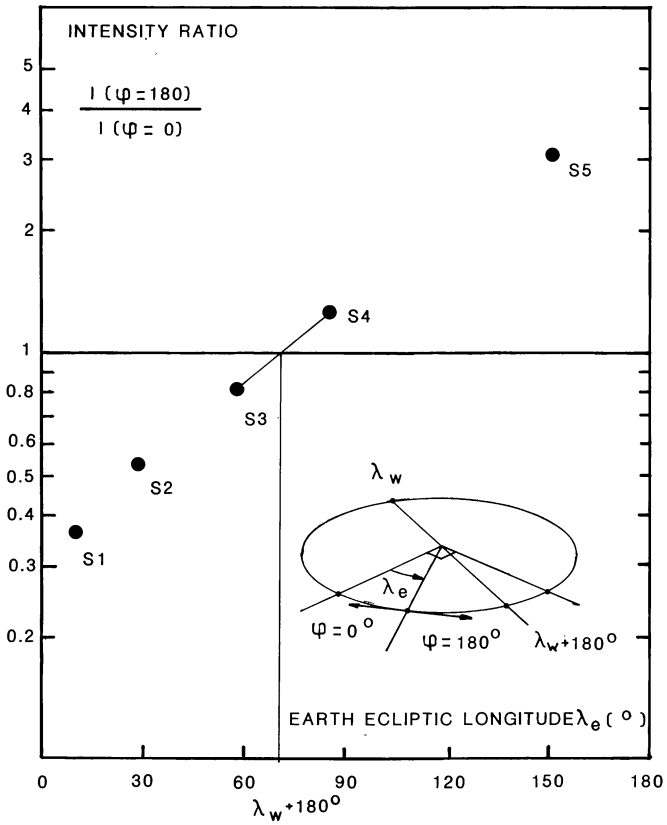

Fig. 10. The ratio of intensities measured for each seance in the ecliptic plane $I(\phi = 180°)/I(\phi = 0°)$ is plotted as a function of ecliptic longitude λ_e. This ratio should be 1 when the spacecraft is at the downwind position DW, for symmetry reasons. Interpolating between S_3 and S_4 points indicate that the longitude of vector $-V_w$ is $71 \pm 2°$. The solar system is moving in respect to the LISM in the opposite direction V_w, at $\lambda_w = 251 \pm 2°$

partially the interplanetary emission (which implies a minimum value of the LISM temperature). Other observations represent intermediate cases.

With the DASS method, we have analyzed individually the absorption throughs of curves $R(\phi)$ for the five observations S_1 to S_5, assuming that the emission line profile was a gaussian. In such a case the value of $R_{\min}$ can be related immediately to a temperature, and the shape of the curve $R(\phi)$ can be used to check that there is no significant galactic contribution superimposed to the interplanetary contribution. We reported (Lallement et al., 1984) that the temperature was varying by $\simeq 3000$ K with location in the solar system, with a systematic increase from upwind to downwind *directions* of observation (regardless of the position of observation).

This was a clear demonstration that the velocity distribution of interstellar hydrogen atoms is modified by interaction with the sun, particularly by ionization and solar gravitation, when it is not exactly balanced by solar Lα radiation pressure. Several authors have modeled this "heating" effect, and Wu and Judge (1980) have calculated emission line profiles for various directions of observations, in order to re-interpret our first estimate of $T = 8800 \pm 1000$ K extracted from a preliminary analysis of PROGNOZ 5 results (Bertaux et al., 1977). As a matter of fact, we found from PROGNOZ observations (Lallement et al., 1984) an increase of the heating effect larger than predicted by the Wu and Judge analysis (1980), especially when the direction of sight was making an angle θ with the upwind direction larger than $\simeq 80°$. However, we analyzed only the direction $\phi(R_{\min})$, where the temperature T is easy to determine since the Doppler Shift is known to be zero, and the θ coverage was somewhat limited. We will come back to this problem later.

What was sure is that, in order to analyze the data in more details, we needed a full model of interaction. It was built to include the effect of ionization and solar radiation pressure, and does not differ basically from the Wu and Judge model (1980), except that it is far more general, since it can handle any location and direction of sight, and values of μ smaller or larger than unity. Such description of the interaction can be referred to as the "classical" theory.

The parameters are:

Dynamical parameters: T, temperature of H in the "unperturbed" LISM.

V_w velocity of the solar system in respect to the LISM (λ_w, β_w, V_w)

$\mu = \frac{F_r}{F_g}$, ratio of solar Lα radiation pressure to gravitation.

Ionization parameter: T_D, lifetime of one H atom placed at 1 AU against photoionization and solar wind charge-exchange. T_D is the inverse of the ionization rate β.

The density n_H at infinity is only a scaling factor for the intensity and plays no role on the reduction factor. The model is stationary.

The influence of the various parameters on the curves $I(\phi)$ and $R(\phi)$ was systematically studied in the companion paper, in order to establish a few guidelines which would help us in the comparison of the full measured curves $R(\phi)$ to the model prediction.

One finding was that the lifetime T_D was modifying the $R(\phi)$ curves substantially when T_D was changed from 0 to a more realistic value $T_D = 2.5\ 10^6$ s but within a reasonable range of values around this average value, the curves $R(\phi)$ were no longer modified by a change of T_D. Therefore, we kept fixed at this value the lifetime T_D for a first estimate of the other parameters.

As mentioned earlier, the direction of the wind was also fixed at the value determined for helium (defined by $\lambda_w = 74.5°$ and $\beta_w = -6°$ for the ecliptic coordinates of the downwind axis), but the value of V_w was set free.

Therefore, we tried to determine from the measured curves $R_m(\phi)$ of Figs. 9a–e the parameters T, μ, and V_w. All three parameters have a combined influence on the value and exact shape of the curves $R(\phi)$.

Thanks to the systematic parametric study of our model, we could try many combinations of these three parameters in a coordinated manner, and the fit to data was estimated visually. However, as it was mentioned at the end of the first section, it was not possible to find a single set of parameters fitting the data in all directions at the same time, as it will be shown below. The upwind hemisphere and the downwind hemisphere could not be fitted simultaneously, but the global fit on the whole sky was much better when the parameters were selected to fit the upwind hemisphere than when they were selected to fit the downwind hemisphere.

This global discrepancy shows most likely a shortcoming in the "classical" theory of the interaction, which should show up more strongly in the downwind hemisphere than in the upwind hemisphere, which is more representative of LISM before interaction with the sun.

Alternatively, the stationarity assumption may not be valid, if variations of solar parameters μ and T_D are substantial. In this case, this assumption is more valid toward the upwind hemisphere than

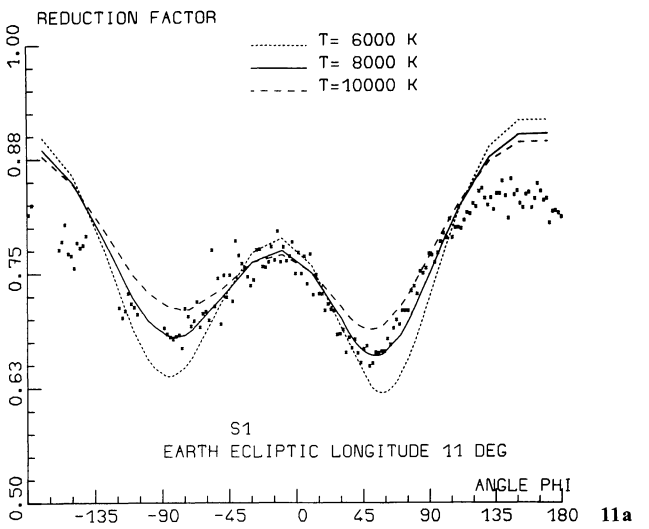

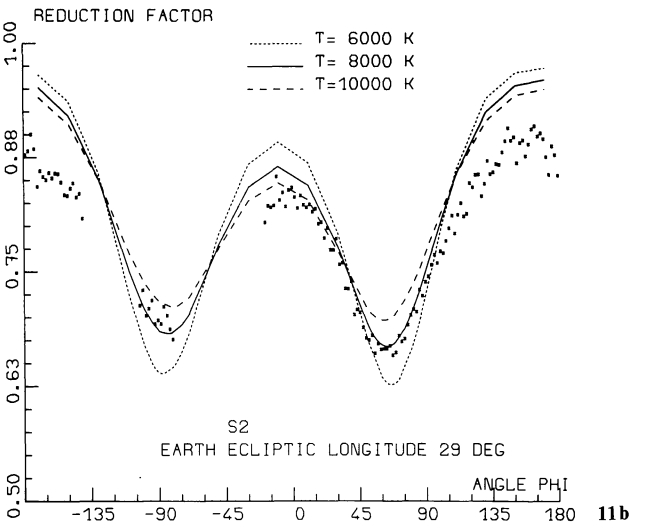

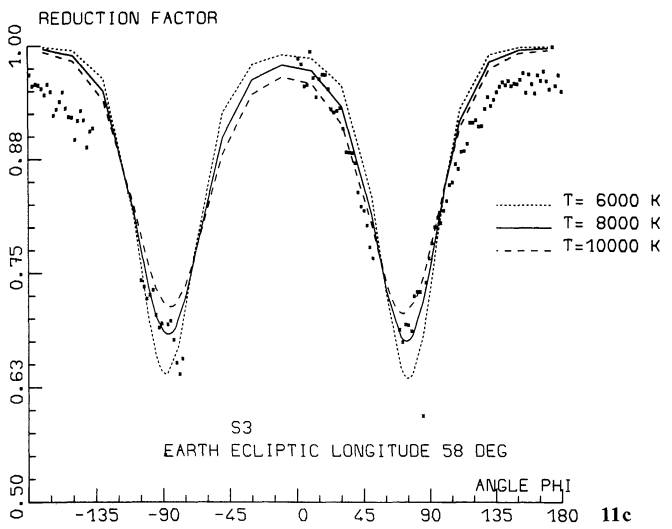

Fig. 11a–c. The measured reduction factor is compared to the model (fully described in the companion paper) for three values of the LISM temperature T and for three observations S_1, S_2, S_3. The value of the minima indicates that $T = 8000 \pm 1000$ K. The overall agreement data/model is quite good, except around $\phi = 180°$. As explained in the text, the measured absorption, larger than predicted (reduction factor smaller), could be explained by heating of H atoms through elastic collisions with solar wind protons, an effect not included in the model. The other parameters are fixed at their best estimated value as determined from the overall comparison data/model

toward the downwind hemisphere, because the line of sight is probing in this last case regions of the solar system where emission is distributed over a longer space scale, corresponding also to a longer time scale.

For all these reasons, we decided to search for the parameters fitting best the upwind hemisphere.

The "best fit" combination of the three parameters was found to be:

$$T = 8000 \pm 1000\,\mathrm{K}$$
$$V_w = 20 \pm 1\,\mathrm{km\,s^{-1}}$$
$$\mu = 0.75 \pm 0.1\,.$$

The uncertainty interval was also determined visually. In Fig. 11a–c, reduction factor data points are compared to theoretical curves $R(\phi)$ for three temperatures, the other parameters V_w and μ being kept fixed at their best estimate.

Overall shape, position of minima $\phi(R_{\min})$, and exact value of $R_{\min}$ are best represented by $T = 8000$ K, whereas $T = 6000$ and 10,000 K are clearly excluded by data points.

However, curves $R(\phi)$ departs seriously from data points in the region $120 \leqq \phi \leqq 240°$ for observations S_1, S_2, S_3. Since they are located before $\lambda_e = 74.5°$, it indicates a systematic departure of data from the model when the direction of sight is approaching the downwind region.

We found some other combinations of parameters which could locally represent better the data around the downwind region, but then the fitting to the upwind region degraded much more seriously, and none of them was really giving a better global fit than the one studied here. Therefore, it seems that something is missing in our interaction model to represent the spectral profile in the downwind direction, which is the region where H atoms have already interacted with the Sun.

The fact that there is more measured absorption than is predicted by the model when $120 \leqq \phi \leqq 240°$ indicates that the emission Lα line is different than predicted by the model. At the present time, we see two possible explanations. One is multiple scattering and the other is a real modification of the velocity distribution. Keller et al. (1981) have made a Monte Carlo calculation of the multiple scattering, indicating that the linewidth might increase by 20%, especially in the downwind direction. But careful calculations have shown that the absorption measurements imply that the observed line shape is different from any one predicted by the model.

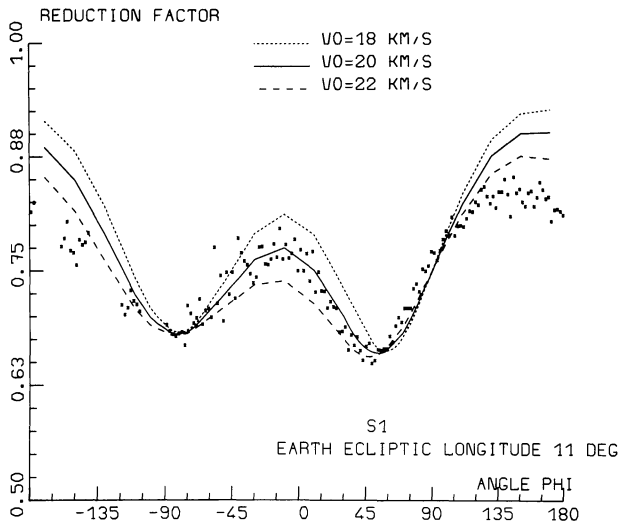

Fig. 12. The measured reduction factor of observation S_1 is compared to models with three values of the velocity. Again, the fit is excellent with $V = 20 \pm 1\,\mathrm{km\,s^{-1}}$, except for the region around $\phi = 180°$, for the same reasons as for the temperature fit of Fig. 11a–c

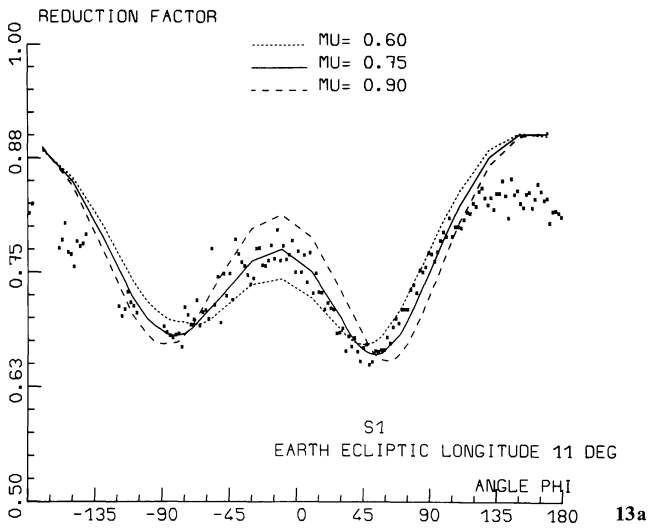

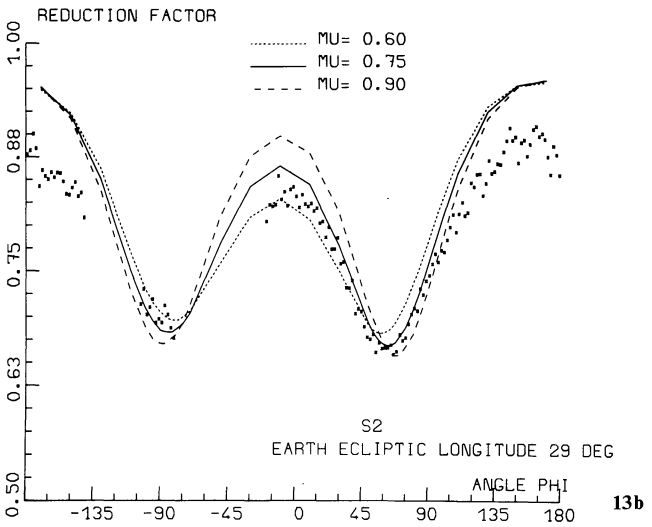

Fig. 13a and b. The measured reduction factor for observations S_1 and S_2 is compared to models with various values of μ, the ratio of solar radiation pressure to gravitation. The best fit of the minima angular positions os obtained for $\mu = 0.75 \pm 0.075$

It can be noticed that, during observation S_5 (Fig. 14e), where the Doppler angular modulation is much larger, the reduction factor reaches unity around the downwind direction ($\phi = 0°$), indicating that the maximum Doppler shift of $\simeq 50\,\mathrm{km\,s^{-1}}$ is enough to separate the emission profile from the H cell absorption, implying a maximum value of the apparent temperature in the downwind region of about 60,000 K.

In fact, if the Doppler shift is not known exactly, a direct linewidth measurement cannot be given with the hydrogen cell method. But a temperature estimate (linewidth measurement) can be given when we are sure that there is no Doppler shift, and such a situation occurs when the reduction factor goes through a minimum value when the sky is scanned. In the preliminary study of the PROGNOZ results with the DASS method restricted to such situations (Lallement et al., 1984), it was found that the temperature (or apparent temperature) was increasing with angle θ (the angle with the upwind direction), as predicted by the "classical" interaction theory and the findings of Wu and Judge (1980). However, it was also found that the measured temperature increase between 80° and 90° (the largest angle explored with this method) was larger than predicted by the classical theory. Our present analysis, more sophisticated, shows that this trend still persists and increases for values of θ larger than 90°.

These findings imply that there might be some additionnal source of heating not included in the model, which would act more in the downwind region; a possible candidate is the elastic collisions between the solar wind and neutral H atoms.

This source of heating could also play a role for helium, which would help to solve the following puzzle: why the helium temperature, determined from the helium cone shape (Dalaudier et al., 1984) is definitely larger ($T(\mathrm{He}) = 16{,}000 \pm 5000$ K) than the hydrogen temperature?

Alternatively, the observed perturbation of the line shape toward the downwind hemisphere could also be the result of a variation of solar parameters over the time scale corresponding to the travel time of H atoms along the emission region in the downwind direction (about $\simeq 4$ AU per year).

Modelling such complicated effects for hydrogen will require an extensive effort much beyond the scope of the present paper, which is mainly focused on the determination of the VLISM parameters, and a further discussion of these findings is for the time being deferred to future.

We also investigated another possibility to explain the departure toward the downwind region by replacing the flat solar line profile by a more realistic one. It is known that there is a self-reversal (Lemaire et al., 1978), which was approximated by a parabola. The effect on the reduction factor was found to be negligibly small, and this possibility was discarded.

We now turn our attention to the parameter V_w. Only observations S_1 and S_2 are sensitive to a variation of this parameter (Fig. 12), because at these positions the relative vector V_r is more or less defined by $V_w - V$, whereas for S_5 it is $V_w + V$. The same variation ΔV_w will change relatively much more $V_w - V$ than $V_w + V$, where V designates the spacecraft velocity.

When only upwind hemisphere data are considered, the velocity is determined to be $V_w = 20 \pm 1\,\mathrm{km\,s^{-1}}$. It agrees pretty well with two previous determinations: $V_w = 19.5 \pm 1.5\,\mathrm{km\,s^{-1}}$

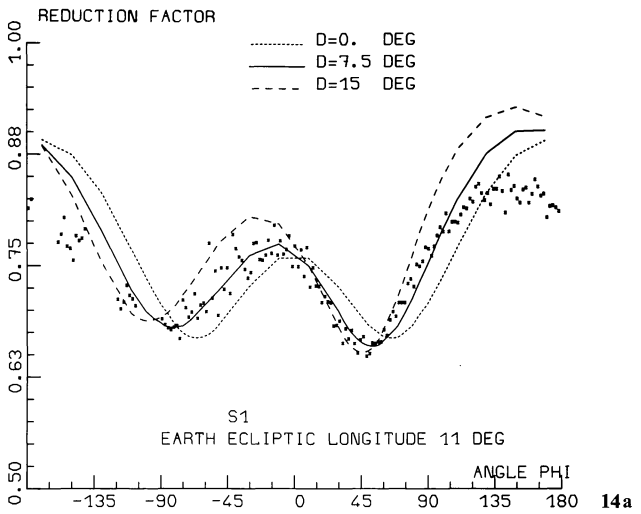

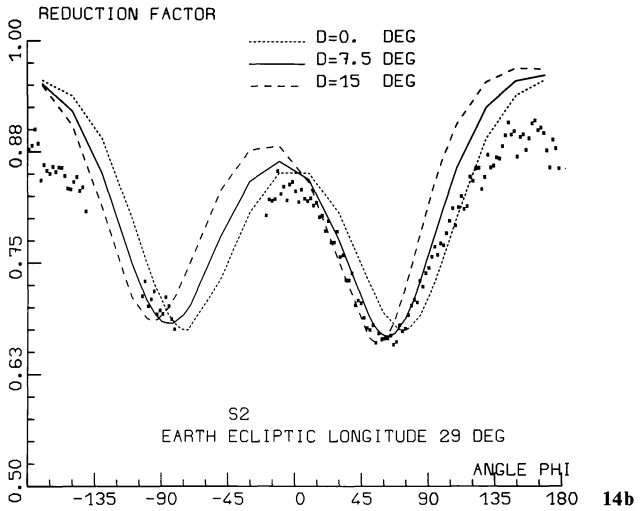

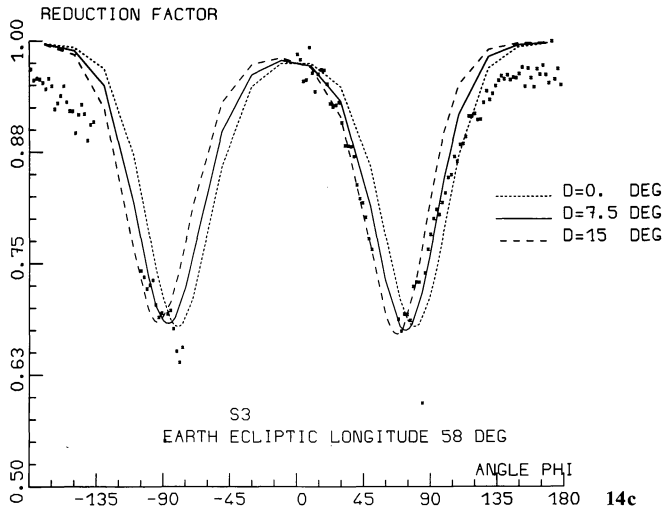

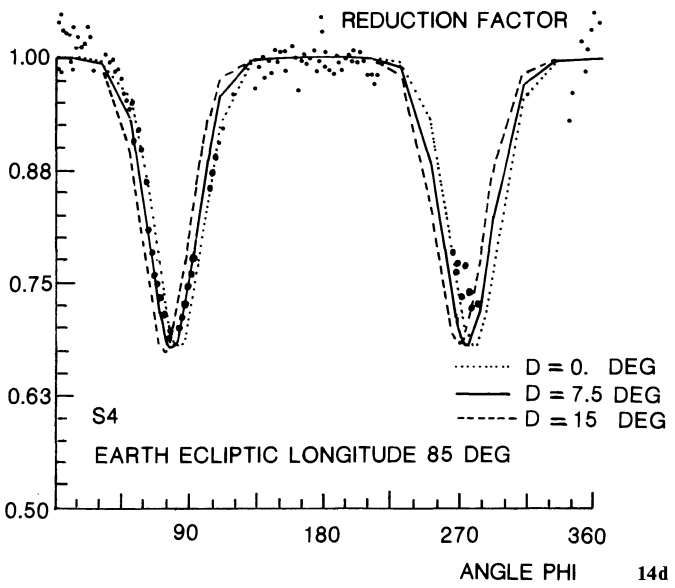

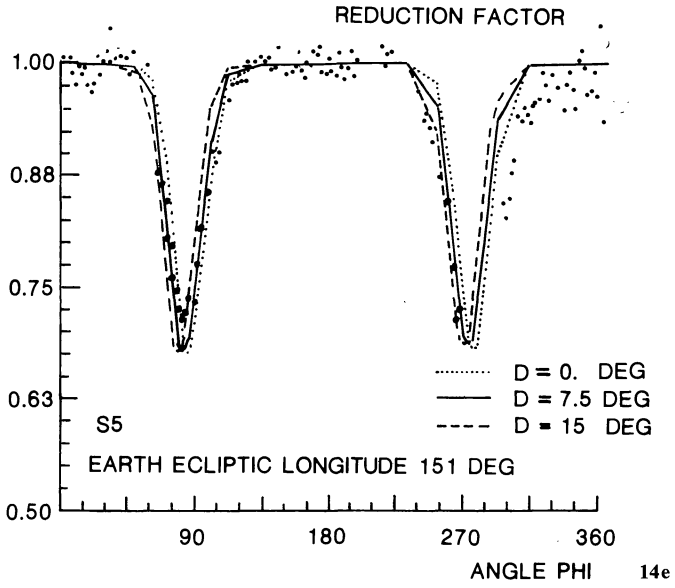

Fig. 14a–e. The measured reduction factor for the five observations S_1 to S_5 is compared to the model with the best fit parameter values, and various values of the ecliptic declination D of vector V_w. The position of the whole measured curves indicates a value of the declination D around $7.5 \pm 3°$. All five seances are sensitive to the exact value of D

from H cell measurements on board the soviet probe Mars 7 (Bertaux et al., 1976) and $V_w = 22 \pm 3\,\mathrm{km\,s^{-1}}$ from Copernicus spectrometric measurements (Adams and Frisch, 1977).

In their analysis, taking into account the modification of the H atoms field velocity by the solar interaction, Wu and Judge (1980) have shown that the *Copernicus* measurement would in fact correspond to $V_w = 19 \pm 3\,\mathrm{km\,s^{-1}}$ and that the earlier PROGNOZ estimate $T = 8800 \pm 1000$ K would rather correspond to $T = 7000 \pm 1200$ K. However, they had to assume a certain direction for the velocity vector V_w, and they selected a limited range of the

parameter μ, from 0.6 to 0.8 (which was good enough at this time since they had only one single PROGNOZ measurement and one single *Copernicus* measurement to interpret), whereas in the present analysis the direction of V_w is determined, and all three parameters V_w, μ, T were scanned systematically and independantly.

In Fig. 13a and b are displayed both data and model curves for various values of μ for observations S_1 and S_2, which contain more information than S_4 and S_5. This is because in this region around the RW ideal position, the total Doppler shift is small enough that there is some absorption by the H cell, whatever is the direction of sight. Therefore, there is everywhere information on the spectral line shape, which is changing continuously from upwind to downwind directions by solar interaction. The exact angular position ϕ at which the reduction factor is minimum is sensitive to μ, as explained in the companion paper.

The value of $\mu = 0.75 \pm 0.1$ provides an absolute determination of the solar Lα flux at line center:

$$F_s = 2.5\ 10^{11}\ \text{phot. cm}^{-2}\text{s}^{-1}\text{Å}^{-1},$$

which is independent of any calibration factor. What is measured is the bending of the individual trajectories of H atoms, under the combined effects of gravitation and Lα radiation pressure.

This value of F_s corresponds to an average over a period of about one year before the measurements, since at 20 km s^{-1}, one H atom travels over 4AU, a distance comparable to the size of the region where the H atoms are emitting and observed.

The present estimate correspond therefore to an average over the period 1975–1976, during solar minimum conditions when R_z solar activity index was below 20.

The ecliptic declination of V_w is determined by comparing models to data for the five observations simultaneously (Fig. 14a–e) and yield a value of $7.5 \pm 3°$, which therefore completes the determination of the vector V_w. In Fig. 14d and e, there is a deviation around $\phi = 0°$ which can reach $\pm 5\%$, slightly larger than usual. However, there are some values of the reduction factor $R \geqq 1$. Since this is impossible by definition of R, it means that the scatter of data in this region is slightly larger than usual too, owing to poorer statistics.

The reduction factor was shown only weakly sensitive to the ionization rate value (in the companion paper) provided it is in a limited range ($2.5\ 10^{-7}$ to 10^{-6} s^{-1}). Thus the whole adjustment was made using an estimated value $\beta = 4\ 10^{-7}$ s^{-1}.

Using the determined values for the dynamical parameters one can therefore use the photometric measurements I_{OFF} to derive by comparison with the photometric model the ionization rate β. The photometric pattern is much influenced by the values of β. However, whatever is β there are systematic departures and the interpretation of the photometric results has required to take into account a non-isotropic solar wind (Lallement et al., 1985). Nevertheless one can give a first approximate value of $\beta \simeq (3 \pm 1)\ 10^{-7}$ s. In the same time the photometric adjustment provides the density "at infinity" if the sensitivity of the photometer is known, since the value of the incident Ly α solar flux has been determined (from the parameter μ). According to a calibration with the hot UV-stars which crossed the field-of-view and to a comparison between the geocoronal signal and a model, we found a density in the range from 0.03 to 0.06 at cm^{-3}.

5. Discussion

Parameters of the LISM derived from the helium cone shape and position (Dalaudier et al., 1984) are compared in Table 2 with the parameters determined from the H cell analysis of interplanetary Lyman-alpha. The direction of the wind are identical within the $\pm 3°$ error boxes. At variance, there is a major discrepancy between Hydrogen and Helium for the modulus velocity V_w and the temperature T and the question arises whether the LISM is a homogeneous medium or not. Since the local mean free path of atoms between collisions is 0.04 pc only, collisions would tend to equalize both the temperature and the velocity modulus of H and He flows, and it is difficult to admit that the discrepancies are of intrinsic origin.

There are unfortunately no helium spectral measurements of sufficient accuracy and the present determination of helium parameters rely only on the interpretation of the photometric pattern. If something is missing in the modeling of the helium flow with the sun, perhaps the derived parameters for helium could be inaccurate.

As pointed out by Lallement (1983) it would require a rather extraordinary coïncidence if the two flows of Helium and Hydrogen had the same direction but different magnitude. As explained in Fig. 15, the velocity V_w of the solar system in respect to the LISM is the composition of the solar motion V_a toward the Apex ($\alpha = 271°$, $\delta = 30°$) in respect to the local standard of reference (LSR) and the motion of the LISM respective to the LSR, the interstellar wind $V_t = V_a - V_w$.

Applying this relationship for H and He separately and subtracting will yield:

$$V_t(\text{He}) - V_t(\text{H}) = V_w(\text{H}) - V_w(\text{He}).$$

Table 2. Characteristics of the VLISM

	Hydrogen	Helium
Velocity module V_w (km s^{-1})	20 ±1	27 ±3
Ecliptic longitude λ_w of V_w (°)	251 ±2	254.5±3
Ecliptic latitude β_w of V_w (°)	7.5±3	6 ±3
Temperature T (°K)	8,000±1,000	16,000±5,000
Density n_∞ (cm^{-3})	3 to 6 10^{-2}	1.5 to 2 10^{-2}

Note: The vector V_w defining the motion of the solar system in respect to the VLISM is opposite to the axis of the helium focusing cone

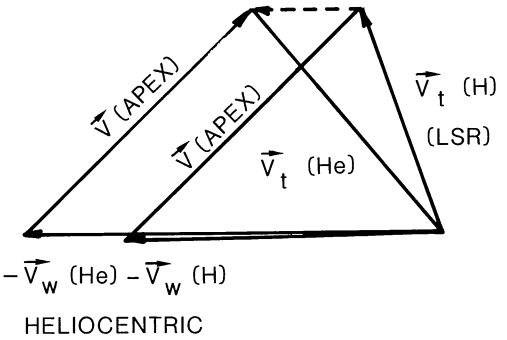

Fig. 15. The motion of the solar system in the LSR is represented by the apex vector V (APEX). The flow of hydrogen and helium in the solar system are $-V_w$(H) and $-V_w$(He). The helium and hydrogen winds in the LSR are V_t(He) and V_t(H). V_w(H) and V_w(He) have the same direction, but seem to have different modulus. Therefore, the difference $V_w(\text{H}) - V_w(\text{He}) \equiv V_t(\text{He}) - V_t(\text{H})$, which is independant of the coordinates system, is parallel to V_w(H), which includes the particular motion of the Sun. This coincidence suggests an artefact in the determination of the modulus of V_w(He)

The difference of intrinsic velocity vector is parallel to V_w(H) $- V_w$(He), which is parallel to both V_w(H) and V_w(He), because they are found to have the same direction. But this direction is imposed by the solar vector V_a, a random vector which is completely independent from the intrinsic difference between H and He interstellar flow.

Therefore, it is likely that the difference of modulus is an artefact of our diagnostic method. Since high resolution spectrometric measurements are quite sensitive to the Doppler shift, we believe that the hydrogen determination is more accurate for the modulus than the photometric determination of the helium velocity.

When considering Fig. 9 of Dalaudier et al. (1984) representing the (V_w, T) parameters giving a good fit to the helium cone shape, it was remarked a certain coupling between V_w and T. If a lower velocity $V_w = 20\,\mathrm{km\,s^{-1}}$ was imposed, perhaps a lower temperature for helium would also result in the fitting process, which would alleviate somewhat the H-He temperature discrepancy too.

Indeed, in a recent study Fahr (1984) suggested that elastic collisions between solar wind protons and helium atoms, which up to now had been ignored, could widen the helium cone, yielding an overestimate of the helium temperature of at least 4000 K if this effect is not taken into account in the modeling. Such an interaction through elastic collisions of solar wind protons could also influence the velocity field of H atoms, particularly in the downwind region, which could explain why the linewidth seen near the downwind direction is larger than expected. A detailed modeling of this effect remains to be done for Hydrogen atoms, but given all these arguments it is our belief that the LISM flow respective to the solar system is characterized by the vector $-V_w$ and the temperature $T = 8000$ K found for hydrogen, and that the discrepance of the helium parameters is only an artefact produced by an imperfect modeling and the shortcomings of the pure photometric method as a means of diagnostic.

The celestial and galactic coordinates of the intrinsic interstellar wind V_t can be computed. As indicated by the $20\,\mathrm{km\,s^{-1}}$ of the hydrogen flow, the motion of the LISM in respect to the local standard frame of reference (LSR) is characterized by a velocity V_t of $16 \pm 1\,\mathrm{km\,s^{-1}}$, whose direction coordinates are:

Celestial coordinates: $\alpha = 14 \pm 3°$ $\quad \delta = 66.5 \pm 3°$

Galactic coordinates: $l_{II} = 124 \pm 3°$ $\quad b_{II} = 4 \pm 3°$.

The ratio of neutral densities n_∞(H)/n_∞(He) is $\simeq 3$, whereas one would expect a cosmological ratio 10. This is easily explained by a substantial ionization of the VLISM. If x is the fraction of ionized hydrogen (we drop ∞ in the following):

$$x = n(\mathrm{H^+})/(n(\mathrm{H}) + n(\mathrm{H^+})) = 1 - n(\mathrm{H})/10n(\mathrm{He})$$

it indicates that $x \simeq 0.7$ in the VLISM, the total density being $n(\mathrm{H^+}) + n(\mathrm{H}) + n(\mathrm{He}) = 0.11\,\mathrm{cm^3}$. Of course, neither $\mathrm{H^+}$ nor $\mathrm{He^+}$ are accessible to studies in the solar system, since they are prevented to enter through the heliosphere.

In the ISM description of McKee and Ostriker (1977) small clouds of dense and cold neutral H ($T = 80$ K, $n = 42\,\mathrm{cm^{-3}}$) are embedded in a hot (10^5–10^6 K) low density ($10^{-2}\,\mathrm{cm^{-3}}$) and totally ionized medium.

According to this model, there is an intermediate phase of the ISM at the interface between the cold and hot phase, composed of two distincts parts, both at 8000 K (warm). The one on the side of the dense cloud is only weakly ionized ($x = 0.15$), and the one on the side of the hot ISM is substantially ionized, with $x = 0.68$, and a total number density of $n = 0.25\,\mathrm{cm^{-3}}$.

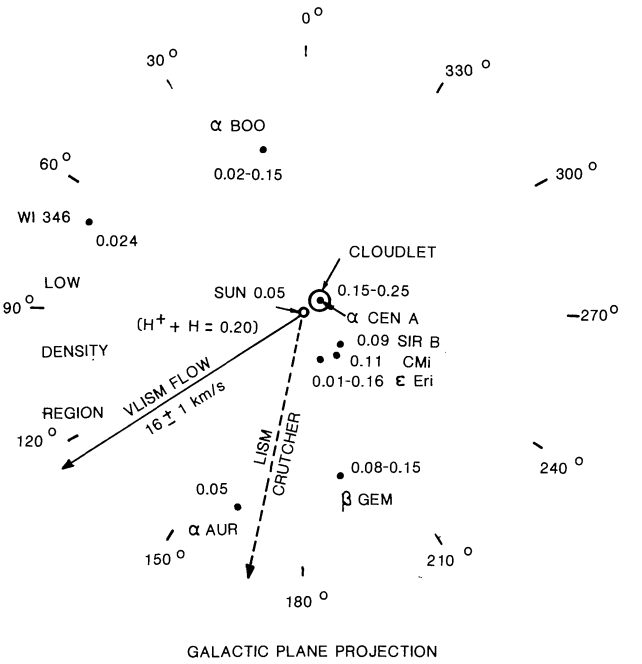

Fig. 16. A few nearby stars (projected on the galactic plane) are shown, together with the average H density measured by interstellar absorption at Lyman-alpha. A possible cloudlet of enhanced density is sketched around α Centauri, toward the region of highest density. The VLISM vector, at $l_{II} = 124°$, is exactly opposite to the direction of α Centauri. It is also significantly different from the LISM flow vector, as determined by Crutcher (1982) from optical interstellar absorption lines within $\simeq 100$ pc, lying at a galactic longitude $l_{II} = 169°$

Though there is some discussion about the number of such cloudlets in the LISM (within $\simeq 100$ pc) (Bruhweiler and Kondo, 1982), the characteristics found for the VLISM: $T = 8000 \pm 1000$ K, $n = 0.11\,\mathrm{cm^{-3}}$ and $x = 0.70$ are strikingly reminiscent of the ionized part of this last interface phase as described by McKee and Ostriker.

Therefore, it would mean that the Sun is presently within $\simeq 2$ pc from a dense cloud. The possibility that such a cloud is moving rapidly in our direction was discussed by Vidal-Madjar et al. (1978), on the ground of Copernicus LISM soundings, D/H distributions and EUV anisotropic radiation pattern. The estimated distance of the dense cloud was 0.03 pc, however, which seems incompatible with the $\simeq 1$ pc thickness of the weakly ionized medium immediately surrounding the cold cloud in the description of McKee and Ostriker (1977), and the strongly ionized medium in which the Sun is moving presently.

Figure 16 is an attempt to compare the characteristics of the VLISM, namely the density and the direction of the VLISM flow, with LISM densities measured on a few nearby stars, either with *Copernicus* or with IUE taken from Vidal-Madjar et al. (1978) and Bruhweiler and Kondo (1982).

If there is a dense cloudlet in the vicinity in the Sun, then it could very well be toward α Cen A, which is the nearest star (1.33 pc) and shows the largest averaged H neutral density of $0.20 \pm 0.05\,\mathrm{cm^{-3}}$ (Dupree et al., 1977). This neutral density is larger than the VLISM by a factor of $\simeq 4$, but is not very different from the total VLISM density ($0.22\,\mathrm{cm^{-3}}$).

One striking feature is that the VLISM flow is exactly opposite to the direction of this enhanced density, and is suggestive of an evoporation mechanism from the cold and dense cloudlet toward the hot and tenuous ISM. It should have therefore a quite local

significance. However, accurate positioning of optical absorption lines on a number of stars in a range of 100 pc (Crutcher, 1982) shows a coherently moving piece of ISM of this scale around the Sun, suggesting that the $\simeq 100$ pc ISM around the Sun could be material which has been shocked and accelerated by stellar winds and super-novae associated with the Scorpio-Ophiucus OB stars, which lies approximately at the opposite of the VLISM flow. But, as indicated in Fig. 16, the VLISM flow is near the galactic plane, at longitude $l_{II} = 124°$, whereas the Crutcher's vector (in respect to LSR) lies at $l_{II} = 169°$. This $\simeq 45°$ difference points again to a local significance for the VLISM flow, justifying the concept of a very Local Interstellar Medium or VLISM, covering a few parsec, with characteristics slightly different from the LISM characteristics, extending over a range of $\simeq 100$ pc. In this respect, the recent detection of a dust cloud in the far infra-red around $l_{II} \simeq 315°$, extended over several tens of degrees (Caux et al., 1984), may confirm the proximity of a moderately dense cloud in the near vicinity of the solar system.

6. Summary

We have reported a series of space measurements of the interplanetary Ly α emission. In addition to the intensity, spectral shape measurements with a hydrogen cell allowed to study the velocity field of H atoms. From this study, scientific information was gathered on three different topics, which are of interest to three different scientific communities:

Basic solar parameters: The bending of the H atoms trajectories is determined from *relative* measurements with the H cell. It needs no calibrated instrument and still yield a quite important absolute value of a solar parameter, the solar Ly α flux at line center $F_s = 2.5 \pm 0.25\ 10^{11}$ phot $(\mathrm{cm^2 \AA s})^{-1}$ for the low solar activity period of 1975–1976.

The decrease of H density along the VLISM flow, which can be measured with an uncalibrated Ly α photometer, allows to measure the absolute value of the ionization rate β, which can be transformed into an absolute determination of the solar wind mass flux at all latitudes by remote sensing.

Interaction processes: The interaction processes between the solar environment and the interstellar medium in which it is embedded, is of broader interest than just solar system studies, since similar interactions can be encountered in other astrophysical condition (i.e., stellar wind expansion).

In addition to the "classical" processes (ionization, solar gravitation, solar radiation pressure) which are included in the most recent models of Wu and Judge and our model, the PROGNOZ observations of unexpected line profiles in the downwind region indicate that something else might be acting on Hydrogen atoms. Elastic collisions with solar wind protons seem an adequate candidate, though a detailed calculation is still to be achieved.

Local Interstellar Medium: Temperature, density and degree of ionization of H atoms (by comparison of H and He densities) indicate that the Sun is presently embedded in an intermediate phase of the ISM, described by McKee and Ostriker as present at the interface of a cold and dense cloud with the hot and tenuous ISM. The accurate determination of the flow vector direction in galactic coordinates shows a significant discrepancy with the vector representing the flow of the LISM over distances of $\simeq 100$ pc, and this points toward a very local significance of the UV observations, justifying the concept of a Very Local Interstellar Medium (VLISM).

Appendix: determination of geocoronal emission

The resonance scattering by the geocoronal H atoms of the solar Ly α gives an additional signal I_g superimposed to the interplanetary background I_p and the measured intensity is $I_m = I_p + I_g$, provided that the line of sight does not intersect the terrestrial disk. The geocoronal intensity is a strongly varying function of the altitudes probed along the line of sight.

If we consider only the problem of the relative intensities, there is effectively a large part of the measurements which can be regarded as free of contamination (the minimum relative contribution I_g/I_m has been found to be about 1 % from the following study). But what is of concern here is the absorption by the H cell, and this will impose more restrictive conditions. As a matter of fact, the geocoronal signal is almost completely absorbed by the cell, whatever is the line of sight for the following reasons. The temperature is much lower ($\leqq 1000$ K which is the temperature at the exobase) than the temperature of the interplanetary hydrogen (8000 K) and the linewidth of the emission is smaller than the bandwidth of absorption. On the other hand there is a very small Doppler shift of the emission since the emitting medium is moving with the earth and the PROGNOZ orbital velocity is less than 2 km s^{-1} for all the measurements used (Fig. 2). As a consequence, even a small contribution to the total intensity is followed by a diminution of the same order of the reduction factor, since all the geocoronal signal is absorbed. If α_g and α_p are the respective proportions of geocoronal and interplanetary intensity ($\alpha_g + \alpha_p = 1$) and if R_g and R_p are the reduction factors respectively for the two emissions the global measured reduction factor will be:

$$R_m = \frac{I_{\mathrm{ON}}}{I_{\mathrm{OFF}}} = \frac{I_{g_{\mathrm{ON}}} + I_{p_{\mathrm{ON}}}}{I_{g_{\mathrm{OFF}}} + I_{p_{\mathrm{OFF}}}} = \frac{R_g I_{g_{\mathrm{OFF}}} + R_p I_{p_{\mathrm{OFF}}}}{I_{g_{\mathrm{OFF}}} + I_{p_{\mathrm{OFF}}}}$$

$$R_m = R_g \alpha_g + R_p \alpha_p .$$

If $R_g \simeq 0$ (nearly complete absorption of the terrestrial signal) then $R_m \simeq R_p \alpha_p$ and 1 % of geocoronal intensity ($\alpha_p = 0.99$) corresponds to 1 % of error if attributing the measured reduction factor to the only interplanetary signal. For example 1 % of error over the reduction factor in the regions of large absorption corresponds to a temperature error of about 350 K or a Doppler velocity error of about 2 km s^{-1} (for the set of parameters that were finally derived) and we would like to avoid such systematic errors.

Thus even for the case of minimal contamination it appears necessary to correct the reduction factor from the influence of the geocoronal absorption to avoid even small, but systematic errors, and that is the reason why the method of correction was applied for all the measurements.

Basic principle of the method

It is represented in a schematic way in Fig. 1A. For a given direction of sight defined by an angle ϕ, one selects all the measurements obtained during the orbital motion of the satellite, in this single direction. As a matter of fact since the spin axis keeps the same orientation only one great circle (of the celestial sphere) is scanned. For a limited interval of time of about 24 h (which corresponds to the fourth part of the PROGNOZ orbital period)

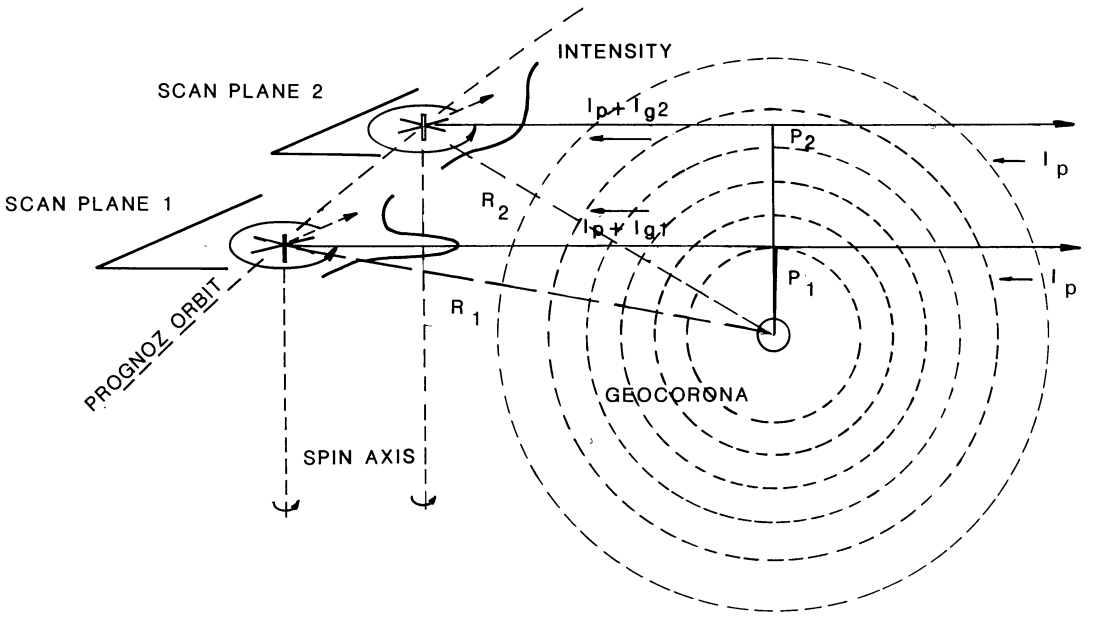

Fig. A1. At two positions along the PROGNOZ orbit, the scan plane of observation cut the geocorona with two different impact parameters $P1$ and $P2$. The measured intensity I_m is the sum of the geocoronal intensity I_g (schematized in each scan plane) and of the interplanetary intensity I_p. For a given angle ϕ, I_p is constant along the trajectory whereas I_g depends on the impact parameter

one can consider that the earth's motion along it own orbit is negligible. Thus the interplanetary background is observed for identical geometrical conditions and the variations of the measured intensity can be attributed to the variations of the terrestrial signal only, superimposed on a constant interplanetary background. Then one can follow the evolution of the geocoronal emission I_g when the geocorona is more and more deeply scanned along the orbital motion of the satellite.

This evolution is compared with the predicted one from a model of geocorona which was constructed by Bertaux in order to analyze the OGO-5 measurements (Bertaux, 1978). This model assumes a classical exospheric distribution (Chamberlain, 1963) without satellite particles contribution. In the "ideal case" of an exact proportionality between the predicted intensity I_t (in Rayleigh) and the measured geocoronal I_g (counts s^{-1}) then for a constant direction we have:

$$I_{\mathrm{OFF}} = I_p + I_g = I_p + a\, I_t, \qquad (1)$$

a being a unique constant including the sensitivity of the photometer (counts s^{-1}) and a coefficient of adjustment to the model, which can be a scaling factor for the geocoronal H density at the exobase level, at 500 km of altitude. The model contains 5 $10^4 cm^{-3}$ atoms at the exobase, and the exospheric temperature is 1000 K.

Whatever the angle ϕ is and which part of the geocorona is scanned, the ratio $\dfrac{I_{2\mathrm{OFF}} - I_{1\mathrm{OFF}}}{I_{t_2} - I_{t_1}}$ calculated for two consecutive measurements, should yield the same value a if the true geocorona was homotetic of the model. Using this value, the I_g and I_p values would be deduced from (1).

There are unfortunately large departures from this "ideal case" as we will see now. For a given angular interval $\Delta\phi$ (of about 10 degrees) the average measured intensities for 5 and 6 consecutive periods (cutting different slices in the geocorona) are compared with the predicted intensities (Fig. A2) and the gradient gives a as a function of angle ϕ (in fact in order to take into account the

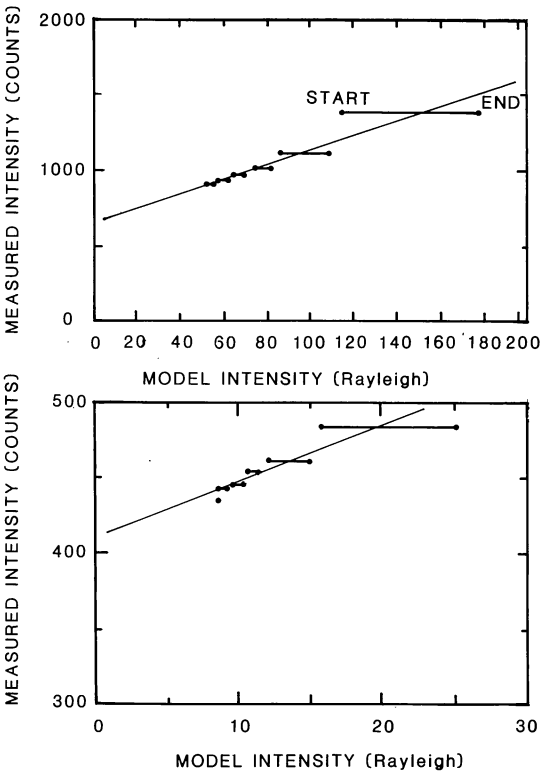

Fig. A2. The total measured I_m (in counts) is plotted as a function of the geocoronal model intensity I_t, for a constant direction of observation ϕ. For each slice of six hours of data, the model intensity (in Rayleigh) was calculated both at the beginning and at the end of the period of six hours, whereas I_m is the measured average over six hours. The slope of the least square straight line is the factor a by which the model has to be multiplied to fit the geocoronal measurements. The two graphs are for two different values of ϕ

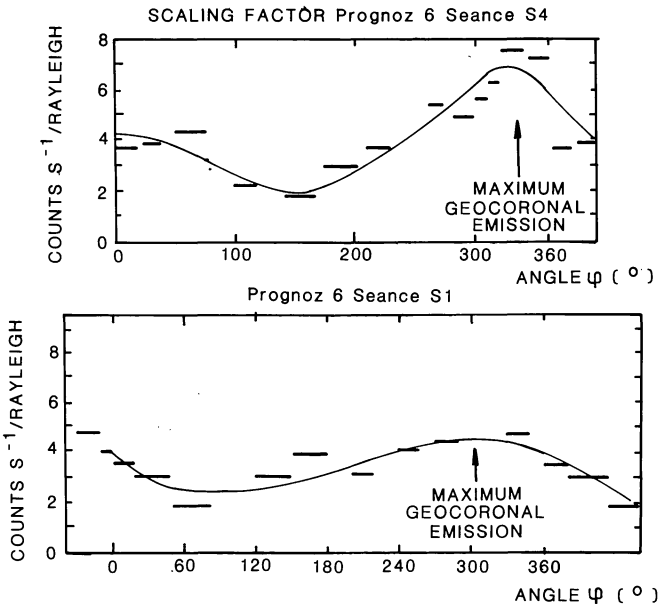

Fig. A3. For two different seances the scaling factor a is plotted as a function of ϕ. If the geocorona were homotetical to the model, a would be a constant, whereas a varies with ϕ and presents a maximum around $\phi = 300°$, where the geocoronal intensity is maximum. The value of a is in counts s^{-1}/Rayleigh, since the geocoronal model predicts intensities in Rayleigh

displacement of the satellite during 6 h the model intensities have been calculated for both the beginning and the end of the 6 h period and the mean value was used). Plots of the gradient a as a function of the spin angle ϕ for seances S_1 and S_4 are shown on Fig. A3.

On each of these it appears than the modulation of a presents a maximum around $\phi = 300°$, corresponding with low impact parameters (and large geocoronal intensities). It means that in the real geocorona, the density decrease with geocentric distance is different from the model prediction.

On the other hand a comparison of the two curves shows, besides this particularity, a different mean level and that is the sign that the two different parts of the geocorona observed during these two seances, do have distinct distributions. In fact if has been shown (Bertaux, 1978) that the geocorona do present some anisotropies which are related to the diurnal variation, even for the external regions ($r \geqq 2\,R_e$).

As a consequence of these departures from the ideal case, this method could not be applied as it was planned initially, and some improvement had to be implemented as follows.

The "variation" method that we used assumed a priori that even if there are some asphericities, the region which is scanned during 5 or 6 consecutive measurements can be considered as "locally" spherical. In addition inside each of these regions we will make the hypothesis that, whatever the position of the satellite and the impact parameter are, the local relation between the true law of decrease of the density and the predicted one implies the existence of a unique biunivocal relation between the measured and predicted intensities. That is this last relation which we will establish empirically separately for each seance. The procedure is the following.

For angle ϕ (or more precisely the mean value of a small interval $\Delta\phi$) the theoretical curves $I_t(\phi)$ show a variation of I_t from two consecutive periods, or "slices", $\Delta I_t = I_{t_2} - I_{t_1}$, which is compared to the measured variation ΔI_{OFF}. The ratio $\alpha = \dfrac{\Delta I_{\mathrm{OFF}}}{\Delta I_t}$ is calculated and affected to the theoretical value $I_t = 1/2\,(I_{t_2} - I_{t_1})$. In a given "bin" of I_t values, various values α coming from different values of ϕ and different pairs of slices were averaged together. Disposing of a total interval for I_t starting from very low value ($\simeq 0$) (that was the case for all the 5 seances) we could then reconstruct "piece by piece" the relation between I_g and I_t by adding the ΔI_{OFF} ($= \Delta I_g$) one after the other, starting from $I_g = 0$ when $I_t = 0$. This kind of integration (it would be a real one if we used infinitesimal variations) is illustrated in Fig. A4.

Tests of validity of the method

The preceding "empirical" relation between I_g and I_t has been defined by using 5 or 6 periods of 6 h, yielding to a single relation for each seance.

Then we calculated the model intensities I_t (in Rayleigh), for all the ϕ values, for every period of 6 h separately, and derived from the established relation $I_g = f(I_t)$ the geocoronal intensity I_g (in count s^{-1}). Finally I_g was subtracted from the measured intensity to yield the "pure" interplanetary background I_p. Since the 5 (or 6) curves $I_p = f(\phi)$ which are so obtained for one single seance are supposed to represent the same background, their intercomparison will provide a test for the validity of the method and will give an idea of the precision that can be achieved. The results for the seance S_1 are shown for example in Fig. 7. The six curves $I_p = f(\phi)$ have been plotted together on the same graph.

There is a good agreement between the different curves. In fact, this method can be reiterated in order to obtain a better agreement, by the progressive adjustment of the relation $I_g = f(I_t)$.

Calculation of the reduction factor

The geocoronal model has been extended to contain the calculation of the Ly α line profile and the absorption by the cell, including also the Doppler shift of the PROGNOZ orbital motion.

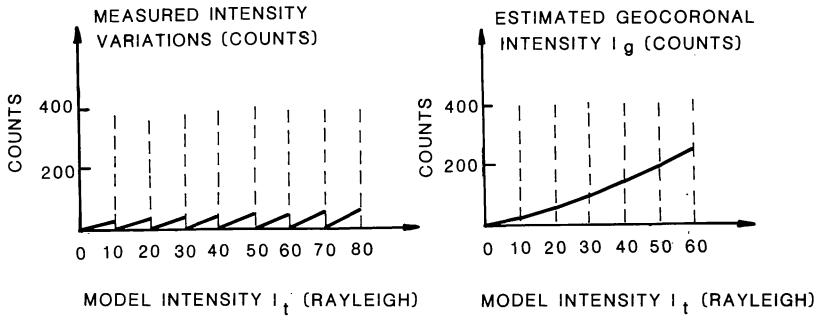

Fig. A4. The method for the establishment of a geocoronal correction is illustrated. On the left side, for each bin of 10 Rayleigh of the model intensity I_t, the measured geocoronal variation is schematized as a small segment. On the right side, all segments are placed on top of each other to find the empirical relationship $I_g = f(I_t)$

Then knowing the respective geocoronal and interplanetary intensities I_g and I_p, and the model absorption factor R_g we can easily deduce the absorption factor R_p on the interplanetary background above, which is related to the measured absorption factor R_m by $R_m = R_p\left(\frac{I_p}{I_g+I_p}\right) + R_g\left(\frac{I_g}{I_g+I_p}\right)$. Like for the intensities the calculation is made for each period of 6 h and the final results are shown on Figs. 9a to 9e, both for intensities and reduction factor. We have eliminated the directions of sight for which the dispersion of the results were too large, corresponding with large geocoronal intensities ($I_g \geqq 300$ Rayleigh).

In future studies, including measurements performed also at lower altitudes, the background will be subtracted from the measurements to yield the pure geocoronal signal for each single measurement (before 6 h averaging) in order to study the geocorona itself.

Acknowledgements. This experiment was a cooperative effort between the Laboratory of UV Astronomy at the Space Research Institute (IKI) of the Academy of Sciences of USSR and the Service d'Aéronomie du CNRS in France. We wish to thank particularly Jean-Francis Brun and Frantz Semelin for developing the experiment and Jean-Claude Lebrun, mathematical engineer, who helped in the data reduction. Paul Feldman is to be thanked for starting our work on stellar observations with this instrument and Bernard Shizgal, for helping us in designing the method for geocoronal correction. CNES (Centre National d'Etudes Spatiales) financed the construction of the experiment and provided computing facilities.

References

Adams, T.F., Frisch, P.C.: 1977, *Astrophys. J.* **212,** 300
Axford, W.I.: 1972, Solar wind, NASA-SP-308, 609
Bertaux, J.L., Blamont, J.E.: 1971, *Astron. Astrophys.* **11,** 200
Bertaux, J.L., Ammar, A., Blamont, J.E.: 1972, *Space Res.* **XII,** 1559
Bertaux, J.L., Blamont, J.E., Mironova, E.N., Kurt, V.G., Bourgin, M.C.: 1977, *Nature* **270,** 156
Bertaux, J.L.: 1978, *Planet. Space Sci.* **26,** 431
Bertaux, J.L., Lallement, R.: 1984, *Astron. Astrophys.* **140,** 230
Blum, P.W., Fahr, M.J.: 1970, *Astron. Astrophys.* **4,** 280
Bohlin, R.C., Savage, B.D., Drake, J.F.: 1978, *Astrophys. J.* **224,** 132
Broadfoot, A.L., Kumar, S.: 1978, *Astrophys. J.* **222,** 1054
Bruhweiler, F.C., Kondo, Y.: 1982, *Astrophys. J.* **259,** 232
Caux, E., Puget, J.L., Serra G., Gispert, R., Ryter, C.: 1985, *Astron. Astrophys.* **144,** 37
Chamberlain, J.W.: 1963, *Planet Space Sci.* 11, 901
Crutcher, R.M.: 1982, *Astrophys. J.* **254,** 82
Dalaudier, F., Bertaux, J.L., Kurt, V.G., Mironova, E.N.: 1984, *Astron. Astrophys.* **134,** 171
Dupree, A.K.: 1975, *Astrophys. J. Letters* **200,** L27
Dupree, A.K., Baliunas, S.L., Shipman, H.L.: 1977, *Astrophys. J.* **218,** 361
Fahr, H.J.: 1974, *Space Sci. Rev.* **15,** 483
Fahr, H.J.: 1985, *Astron. Astrophys.* **142,** 476
Holzer, T.E.: 1977, *Rev. Geophys. Space Phys.* **15,** 467
Keller, H.U., Richter, K., Thomas, G.E.: 1981, *Astron. Astrophys.* **102,** 415
Lallement, R., Bertaux, J.L., Kurt, V.G., Mironova, E.N.: 1984, *Astron. Astrophys.* **140,** 243
Lallement, R.: 1983, Thèse de 3ème Cycle, Université P. et M. Curie, Paris
Lallement, R., Bertaux, J.L., Dalaudier, F.: 1985a, *Astron. Astrophys.* **150,** 21
Lallement, R., Bertaux, J.L., Kurt, V.G.: 1985b, *Journal Geophys. Res.* **90,** 1413
Lemaire, P., Charra, J., Jouchoux, A., Vidal-Madjar, A., Artzner, G.E., Vial, J.G., Bonnet, R.M., Skumanich, A.: 1978, *Astrophys. J. Letters* **223,** L55
McClintock, W., Henry, R.C., Moos, H.W.: 1976, *Astrophys. J. Letters* **24,** L103
McKee, C.F., Ostriker, J.P.: 1977, *Astrophys. J.* **218,** 148
Moos, H.W., Linsky, J.L., Henry, R.C., McClintock, W.: 1974, *Astrophys. J.* **188,** L93
Thomas, G.E., Krassa, R.F.: 1971, *Astron. Astrophys.* **11,** 218
Thomas, G.E.: 1978, *Ann. Rev. Earth Planet. Sci.* **6,** 173
Vidal-Madjar, A., Laurent, C., Bruston, P., Audouze, J.: 1978, *Astrophys. J.* **223,** 589
Weller, C.S., Meier, R.R.: 1974, *Astrophys. J.* **193,** 471
Wu, F.M., Judge, D.L.: 1980, *Astrophys. J.* **239,** 389